Revision 2

The catalytic effect of bound extracellular polymeric substances excreted by anaerobic microorganisms on Ca-Mg carbonate precipitation: Implications for the "dolomite problem"

Fangfu Zhang,[1,†] Huifang Xu,[1,*] Evgenya S. Shelobolina,[1] Hiromi Konishi,[1,‡] Brandon Converse,[1] Zhizhang Shen,[1] and Eric E. Roden[1]

[1]NASA Astrobiology Institute, Department of Geoscience, University of Wisconsin-Madison Madison, WI 53706

[†]Present address: Brine Chemistry Consortium, Department of Civil and Environment Engineering, Rice University, Houston, TX 77005

[‡]Present address: Department of Geology, Niigata University, 8050 Ikarashi 2-no-cho, Nishi-ku, Niigata 950-2181, Japan.

*Corresponding author: Prof. Huifang Xu
Department of Geoscience
University of Wisconsin-Madison
1215 West Dayton Street, A352 Weeks Hall
Madison, Wisconsin 53706
Tel: 1-608-265-5887
Fax: 1-608-262-0693
Email: hfxu@geology.wisc.edu

ABSTRACT

Because of its rare occurrence in modern sediments, as well as the difficulty in synthesizing it under low-temperature conditions in the laboratory, the origin of sedimentary dolomite has remained a long-standing enigma, often referred to as the “dolomite problem”. Recently, anaerobic microorganisms, such as sulfate-reducing bacteria and methanogens, have been recognized for mediating dolomite precipitation. However, the exact role of microorganisms in dolomite crystallization is still under debate and the possible involvement of anaerobic fermenting bacteria has not been studied. In this study, we characterized the effect of purified non-metabolizing biomass and bound extracellular polymeric substances (EPS) of a natural consortium of anaerobic microorganisms dominated by fermenting bacteria and sulfate-reducing bacteria on Ca-Mg carbonate precipitation. This natural consortium was enriched from sediments of Deep Springs Lake, California, where dolomite is still precipitating. Our data show that disordered dolomite, a precursor of some sedimentary stoichiometric ordered dolomite, can be precipitated in calcite-seeded Ca-Mg carbonate solutions containing purified non-metabolizing consortium biomass. Bound EPS extracted from the consortium culture were shown to be the active component that triggered the crystallization of disordered dolomite. Further experiments show that purified non-metabolizing biomass from pure cultures of both anaerobic fermenting and sulfate-reducing bacteria closely related to those organisms present in the consortium could also catalyze the precipitation of disordered dolomite. This study contributes to the understanding of the “dolomite problem” by revealing (1) the catalytic effect of bound EPS on Ca-Mg carbonate crystallization and (2) the possible involvement of anaerobic fermenting bacteria in sedimentary dolomite formation, which has not been reported previously.

Keywords: Disordered dolomite, dolomite problem, sulfate-reducing bacteria, fermenting bacteria, non-metabolizing biomass, bound EPS

INTRODUCTION

The formation mechanism of dolomite has long been a controversy, commonly referred to as the "dolomite problem" (Hardie 1987; Machel and Mountjoy 1986; Mazzullo 2000; Warren 2000; Zenger et al. 1980). Dolomite is rare in Holocene and modern sediments, yet abundant in older rocks. According to thermodynamics, aqueous solutions supersaturated with respect to dolomite, such as seawater, certain lake waters, many groundwaters, and hypersaline waters are theoretically capable of precipitating dolomite as cement or dolomitizing limestone; however, such cases are rare in modern carbonate environments (Hardie 1987). Moreover, extensive attempts to synthesize dolomite inorganically under Earth-surface conditions have been unsuccessful (Land 1998).

The observation of dolomite occurrence within some anoxic, organic-rich sediments as a result of anaerobic microorganisms has provided a new biogeochemical approach to solving the "dolomite problem" (Baker and Burns 1985; Bontognali et al. 2010; Compton 1988; Deng et al. 2010; Mazzullo 2000; Roberts et al. 2004; Vasconcelos and McKenzie 1997; Wright 1999). Following this observation, laboratory syntheses of Ca-Mg carbonates in live cultures of sulfate-reducing bacteria (SRB) or methanogens have been conducted to study the effect of microorganisms on carbonate precipitation (Deng et al. 2010; Kenward et al. 2009; Van Lith et al. 2003b; Vasconcelos et al. 1995; Warthmann et al. 2000; Wright and Wacey 2005). However, the possible involvement of anaerobic fermenting bacteria in sedimentary dolomite formation

has been largely ignored. Fermenting bacteria play a critical role in the cycling of some organic compounds in an ecosystem or a biofilm. For example, SRB depend on some products of fermenting bacteria which they can respire to CO_2 (Jørgensen 2000). Considering the importance of fermenting bacteria in anoxic environments, the role of fermenting bacteria in dolomite formation warrants more attention.

In addition, despite a number of studies on microbe-related dolomite precipitation, the exact role of microbes is still not clear. The involvement of EPS in carbonate precipitation has been reported. For example, since EPS carries negative charges that are able to bind and accumulate metal cations, EPS has been frequently considered as providing sites for carbonate nucleation (Aloisi et al. 2006; Benzerara et al. 2006; Bosak and Newman 2005; Braissant et al. 2007; Gautret et al. 2004; Kawaguchi and Decho 2002). Previous laboratory dolomite precipitation experiments within live cultures of SRB and methanogen have also suggested the involvement of EPS in promoting dolomite nucleation and growth (Bontognali et al. 2014; Bontognali et al. 2008; Goldsmith and Graf 1958; Kenward et al. 2009; Roberts et al. 2004; Van Lith et al. 2003a; Van Lith et al. 2003b). However, within live cultures, it is difficult to define the components that actually mediate dolomite crystallization, as microbes, microbial metabolic products, and the complex ingredients of typical culture media may all affect carbonate precipitation. For example, phosphate in culture media can lead to the precipitation of Ca/Mg-phosphate minerals. It also has a pronounced impact on carbonate precipitation and can potentially obscure or alter more subtle effects on mineral precipitation, which might lead to misinterpretation of culture studies meant to simulate natural systems (Gallagher et al. 2013).

In this paper, we cultured a natural consortium of anaerobic microorganisms in the laboratory and investigated the effect of their non-metabolizing biomass and bound EPS on

dolomite crystallization. By definition, bound EPS is associated with the cell surface and includes sheaths, capsular polymers, condensed gel, loosely bound polymers, and attached organic materials, while soluble EPS, including soluble macromolecules, colloids, and slimes, is loosely associated with the cells and predominantly generated by sloughing off from bound EPS (Hsieh et al. 1994; Laspidou and Rittmann 2002; Nielsen et al. 1997). The consortium was enriched from pore fluids of Deep Springs Lake, a highly alkaline playa lake in California where dolomite is still precipitating (Jones 1965; Meister et al. 2011). To avoid the possible influence of the components of cultures, an experimental procedure which used purified non-metabolizing consortium biomass and bound EPS-bearing solutions was employed. To determine the microorganisms in the consortium whose bound EPS was likely to have promoted the precipitation of disordered dolomite, biomass from pure cultures obtained from culture collection was evaluated in a similar manner. These included anaerobic fermenting bacteria (*Halanaerobium saccharolyticum* subsp. *saccharolyticum* corrig. strain DSM 6643) and SRB (*Desulfohalobium retbaense* strain DSM 5692), which are closely related to those organisms present in the consortium.

MATERIALS AND METHODS

Microorganisms and culture medium

Pore fluids were collected from Deep Springs Lake, California and an anaerobic microbial consortium were enriched from pore fluids. Deep Springs Lake is a highly alkaline playa lake in eastern California showing ongoing dolomite authigenesis. The lake water chemistry is characterized by high salinity, pH (9.1-9.6), and dissolved inorganic carbon (DIC),

113 although the solute concentrations strongly vary between the dry and wet seasons and also
114 throughout the years (Jones 1965: Meister et al. 2011). Reported concentrations of Na^+ vary from
115 930 to 6000 mM, Cl^- 460 to 4000 mM, DIC 50 to 600 mM, SO_4^{2-} 130 to 1600 mM, Ca^{2+} 0 to
116 0.45 mM, Mg^{2+} 0 to 2.2 mM, Mg/Ca ratio 0.8 to 8 (Jones 1965: Meister et al. 2011). To match
117 the lake water chemistry, we used a modified selective alkaline medium (Zhilina et al. 1997) to
118 culture the consortium. This medium contained ~ 2123 mM Na^+, ~ 1731 mM Cl^-, ~ 273 mM
119 DIC, and ~ 21 mM SO_4^{2-}. Measured pH of the medium was 9.4-9.5. Overall, the medium
120 chemistry was similar to that of lake water, although the SO_4^{2-} concentration was lower. The
121 consortium has been growing well in this medium. Detailed components of this medium were:
122 $NaHCO_3$ 15 g/L, Na_2CO_3 10 g/L, NaCl 100 g/L, NH_4Cl 1 g/L, KCl 0.2 g/L, K_2HPO_4 0.2 g/L,
123 Na_2SO_4 3 g/L, Na_2S 0.25 g/L, yeast extract 0.5 g/L, 10 ml/L of a vitamin solution (Wolin et al.
124 1963), 1 ml/L of a trace element solution (Whitman et al. 1982) and H_2 as electron donor. Na_2S
125 was added separately from a sterile stock solution after the medium was autoclaved.

126 16S rRNA gene amplicon sequencing was used to identify dominant microorganisms in
127 the consortium culture. Culture DNA was isolated using the UltraClean Soil DNA Isolation Kit
128 (MoBio Laboratories Inc, 2746 Loker Ave West, Carlsbad, CA, 92010). Total DNA from the
129 enrichment culture was polymerase chain reaction-amplified using primers targeting variable
130 regions 1 through 2 of the bacterial 16S rRNA gene (V1-2), gel purified, and sequenced using
131 454/Roche GS FLX technology (Liu et al. 2007). Raw sequence data was analyzed using QIIME
132 (Caporaso et al. 2010) with default settings. Classification was performed within QIIME using
133 the Ribosomal Database Pipeline (RDP) (Wang et al. 2007), and BLAST (Altschul et al. 1990)
134 was used to further classify the abundant sequences.

Halanaerobium saccharolyticum subsp. *saccharolyticum* corrig. strain DSM 6643 is a gram-negative, anaerobic, fermentative, and halophilic bacterium (Rainey et al. 1995; Zhilina et al. 1992). The medium used for culturing this strain was a modified Medium 591 (German Collection of Microorganisms and Cell cultures), containing: NH_4Cl 0.33 g/L, $CaCl_2$ 0.33 g/L, $MgCl_2$ 0.33 g/L, KCl 0.33 g/L, KH_2PO_4 0.33 g/L, NaCl 100 g/L, $NaHCO_3$ 1.50 g/L, $Na_2S•9H_2O$ 0.50 g/L, glucose 5.00 g/L, peptone 5.00 g/L, 10 ml/L of a vitamin solution (Wolin et al. 1963), and 1 ml/L of a trace element solution (Whitman et al. 1982). The medium was prepared under a N_2:CO_2 (80:20 v/v) atmosphere. The pH of the medium was adjusted to 7.5 with a NaOH solution. $NaHCO_3$, Na_2S, glucose, and peptone were added separately from sterile stock solutions after the medium was autoclaved. The stock solution of $NaHCO_3$ was prepared under a N_2:CO_2 (80:20 v/v) atmosphere, while those of Na_2S, glucose, and peptone were under 100% N_2.

Desulfohalobium retbaense strain DSM 5692 is a gram-negative, sulfate-reducing bacterium isolated from sediments of a hypersaline lake in Senegal, with the optimum temperature for growth of 37 to 40 °C (Ollivier et al. 1991). The medium used for culturing this strain was a modified Medium 499, containing: NH_4Cl 1 g/L, K_2HPO_4 0.3 g/L, KH_2PO_4 0.3 g/L, $MgCl_2•6H_2O$ 20.0 g/L, NaCl 100 g/L, $CaCl_2•2H_2O$ 2.7 g/L, KCl 4.0 g/L, Na_2SO_4 3 g/L, Na-acetate 1.0 g/L, trypticase 1.0 g/L, yeast extract 1.0 g/L, Na-(L)-lactate 2.5 g/L, Na_2S 0.3 g/L, 10 ml/L of a vitamin solution (Wolin et al. 1963), and 1 ml/L of a trace element solution (Whitman et al. 1982). The medium was prepared under 100% N_2. The pH of the medium was adjusted to 7.0 with a NaOH solution. K_2HPO_4, KH_2PO_4, Na-acetate, trypticase, yeast extract, Na-(L)-lactate, and Na_2S were added separately from sterile stock solutions prepared under 100% N_2 after the medium was autoclaved.

158 **Biomass collection**

159 Since the consortium enrichment culture was enriched from the lake pore fluids which
160 may contain small amounts of dolomite from lake sediments, the consortium culture was
161 transferred for 8 generations before biomass collection so that precipitates from carbonate
162 precipitation experiments with consortium biomass will not be contaminated by dolomite from
163 lake sediments.

164 All the cultures were incubated at 37 °C and growth of cultures was monitored from time
165 to time by measuring optical density. The consortium culture reached the stationary phase
166 between 5-7 days after inoculation. For *H. saccharolyticum* and *D. retbaense* cultures, it was 3-5
167 days. In the early stationary growth phase, biomass from the consortium culture and both model
168 cultures was collected. The pH of the cultures at collection was 8.9-9.0, 5.4-5.5, and 7.0 for the
169 consortium**,** *H. saccharolyticum* and *D. retbaense*, respectively. No precipitates were observed in
170 either live cultures or cell-free medium. Cultures were first centrifuged at 20,000 G for 20 min
171 with a Beckman-Coulter Avanti® J-E centrifuge to concentrate the biomass. Subsequently, the
172 biomass was washed with a N_2-sparged washing buffer containing all the inorganic ingredients
173 in the medium but not the organic ingredients to remove the possible residue organics from the
174 medium and other soluble microbial metabolites. The reason to use such a washing buffer was
175 that it carried an ionic strength and composition similar to that of the medium; otherwise some
176 bound EPS components might desorb and thus be washed away from the EPS matrix (Nielsen
177 and Jahn 1999). The washing buffer with the biomass was centrifuged at 20,000 G for 20 min
178 and the supernatant was discarded. After that, 60 ml of washing buffer was added to the washed
179 biomass, which was then dialyzed against ~ 6 L of distilled de-ionized (DI) water before used for
180 further carbonate precipitation experiments. During the dialysis, the DI water was changed for 3

times. Due to the diffusion of water into the dialysis bag, the volume of the biomass solution expanded significantly. The volume of the biomass solution stopped increasing ~ 16 h after dialysis started, indicating that 16 h was long enough for the dialysis. To make sure that the dialysis was complete, all the biomass solution was dialyzed for 24 h. The biomass was metabolically non-metabolizing after dialysis since it was exposed to air during dialysis. After dialysis, we usually collected ~ 120 ml of biomass solution out of ~ 3 L of culture. To obtain the concentration of biomass in solution, a portion of biomass solution was freeze-dried at -50 °C for 48 h for measuring the dry weight.

Extraction and Characterization of bound EPS of the anaerobic microbial consortium

The bound EPS of the anaerobic microbial consortium was extracted in the early stationary growth phase. Biomass of the anaerobic microbial consortium was concentrated and washed following the aforementioned procedure. Subsequently, a certain volume of washing buffer was added to the washed biomass to obtain a biomass concentration of 2 mg/mL and bound EPS was extracted from this biomass solution following a previously established procedure using formaldehyde with NaOH developed for anaerobic sludges (Liu and Fang 2002). After dialysis, we can usually collect ~ 90 ml bound EPS solution out of ~ 3 L of consortium culture. To determine the concentration of bound EPS in solution, a portion of bound EPS solution was freeze-dried at -50 °C for 48 h for measuring the dry weight of bound EPS. The residue dead cell pellets (DCP) after bound EPS extraction were also collected by adding a certain amount of washing buffer to the residue pellets and dialysis against DI water for 24 h.

The total carbohydrate content of bound EPS was measured using a modified phenol-sulfuric acid method with glucose standards (Dubois et al. 1956). Polysaccharides (or other

monomeric sugars in EPS) were first hydrolyzed to individual monosaccharides with H_2SO_4 (Pakulski and Benner 1992). To do this, 1 mg of dry EPS was added into 1 mL of 12 M H_2SO_4 at room temperature for 2 h. Then 9 mL DI water was added into the slurry. Samples were briefly (3-5 s) ultrasonicated to promote the dissolution of the residue. A 5 mL aliquot of the solution was pipetted into a 50 mL serum vial, crimp-sealed with Teflon liners and hydrolyzed at 100 °C for 3 h. Then 1 mL aliquot was added into a test tube followed by 1 mL of phenol solution (5%) and 5 mL of 98% sulfuric acid. The tube was shaken vigorously on a shaker. After 10 min, it was placed in a water bath at 30 °C for 20 min. The mixture was cooled and measured for absorbance at 490 nm using an UV-Vis spectrophotometer (UV-mini 1240, Shimadzu Corp, Kyoto, Japan). The final results were normalized by the dry weight of bound EPS. Bound EPS collected from three batches of the culture was analyzed and duplicate aliquots were analyzed for each bound EPS sample. All experimental glassware used in these analyses was acid washed, rinsed with DI water, and combusted at 550 °C for 6 h to prevent the possible organic contamination.

The sugar monomer composition of intact bound EPS was measured through glycosyl analyses using gas chromatography combined mass spectrometry (GC/MS) of the per-O-trimethylsilyl (TMS) derivatives of the monosaccharide methyl glycosides produced from the sample by acidic methanolysis. 400 μg of the sample was used for the analysis. 20 μg of inositol was added to the sample as an internal standard. Methyl glycosides were then prepared from the dry sample by methanolysis in 1 M HCl in methanol at 80 °C (18 h), followed by re-N-acetylation with pyridine and acetic anhydride in methanol (for detection of amino sugars). The sample was then per-O-trimethylsilylated by treatment with Tri-Sil (Pierce) at 80 °C (0.5 h). These procedures were carried out as previously described (Merkle and Poppe 1994; York et al. 1986). GC/MS analysis of the TMS methyl glycosides was performed on an Agilent 6890N GC

interfaced to a 5975B MSD, using an Agilent DB-1 fused silica capillary column (30 m × 0.25 mm ID).

Carbonate precipitation experiments with the non-metabolizing consortium biomass, bound EPS of consortium, DCP with bound EPS removed

All carbonate precipitation experiments were carried out at room temperature and at least in duplicates. Solutions containing non-metabolizing consortium biomass/bound EPS/DCP were diluted with DI water to obtain the desired concentration **(Table 1 and 2)**. Then reagent grade $CaCl_2 \cdot 2H_2O$ and $MgCl_2 \cdot 6H_2O$ and calcite seeds (0.2 g/L) were added into solution. The concentration of $CaCl_2$ in solution was fixed at 10 mM with variable $MgCl_2$ concentration (30, 50, and 80 mM) to produce different Mg:Ca ratios (3:1, 5:1, and 8:1). Calcite crystals prepared by grinding a chunk of chalk sample were used as seeds for heterogeneous nucleation (Zhang et al. 2012a; Zhang et al. 2012b). The specific surface area of the resulting chalk seeds, as determined by the multipoint N_2-BET method, is 2.8 m^2/g.

Experimental solutions were ultrasonicated for 5 min to suspend chalk seeds and then left still for overnight so that solutions could be equilibrated with atmospheric CO_2 and chalk seeds. After that, the pH of experimental solutions was measured as the initial pH. A geochemical program (PHREEQC) was used to calculate the starting chemical compositions of the control solutions (Parkhurst and Appelo 1999). The starting pH of the control solutions and PHREEQC calculations suggests that approximately 0.035 g/L out of the 0.2 g/L chalk seeds were dissolved and control solutions were equilibrated with atmospheric CO_2. Carbonate precipitation experiments were conducted with a NH_4HCO_3 free-drift method. To do that, experimental solutions were distributed into glass Petri dishes which were placed in a desiccation cabinet

(dimensions 36 × 36 × 41 cm) containing NH_4HCO_3 powders (5 g for a total experimental solution volume of 500 mL). The decomposition of NH_4HCO_3 produces NH_3, CO_2, and H_2O. The dissolution of NH_3 into experimental solutions increased the solution pH and CO_2 dissolution provided CO_3^{2-} source, which can thereby induce carbonate precipitation. In most experiments, precipitates were sampled after 14 days. In some experiments, to study the precipitation process, precipitates were collected after 3, 7, 10, and 14 days. When sampling, precipitates were spun down at 20,000 G for 15 min. The supernatant was discarded and ~5 ml of DI water was added to wash precipitates followed by centrifugation for another 10 min and removal of the DI water. Precipitates were then washed with DI water for several times and then air-dried. The concentrations of Ca^{2+} and Mg^{2+} in solutions both before and after experiments were measured with inductively coupled plasma atomic emission spectroscopy (ICP-AES, Varian Vista-MPX, Australia). Measurements were conducted in duplicates or triplicates for each experimental condition. Parallel control experiments were carried out with organic-free solutions containing only $CaCl_2$, $MgCl_2$, and chalk seeds. Detailed chemical conditions employed in carbonate precipitation experiments are listed in **Table 1**.

Carbonate precipitation experiments with non-metabolizing biomass of *H. saccharolyticum* and *D. retbaense*

Carbonate synthesis experiments were also conducted with *H. saccharolyticum* and *D. retbaense* biomass at room temperature. The experimental procedure was the same as that with consortium biomass except that the concentration of $CaCl_2$ in solutions was fixed at 5 mM, instead of 10 mM, to assure that the catalytic effect of the non-metabolizing biomass was not tied to one condition. The initial Mg:Ca ratios in solution were 2:1, 3:1, 5:1, and 8:1, respectively. In

addition, a synthetic calcite seed (0.2 g/L) was used instead of chalk. The reason to use a synthetic seed was that miniscule amounts of organic materials were found to remain associated with the chalk surface and act as an inhibitor for chalk recrystallization (Belova et al. 2012). Therefore by using synthetic seeds, the possibility can be excluded that the Ca-Mg carbonate precipitation was catalyzed by the organic materials on chalk surface. The synthetic seeds were synthesized by mixing equal volume amounts of 500 mM $CaCl_2$ and 500 mM $NaHCO_3$. X-ray diffraction (XRD) analyses show that calcite was the only phase in the synthetic seeds. SEM studies show that the size of synthetic seeds was usually several microns. The specific surface area of the seed crystals was 0.2 m^2/g. Detailed chemical conditions employed in carbonate precipitation experiments are listed in **Table 2**.

Characterization of synthetic carbonates

XRD, transmission electron microscopy (TEM), and selected-area electron diffraction (SAED) were utilized to characterize synthetic carbonates. Detailed procedures can be found in (Zhang et al. 2012a; Zhang et al. 2012b). SEM samples were prepared by dispersing powders on carbon tapes. SEM observations were performed using a Hitachi S3400 SEM and a LEO 1530 SEM. Both were equipped with energy dispersive spectroscopy (EDS) capabilities to characterize the solid-phase composition. Samples analyzed with Hitachi S3400 were not carbon-coated and observations were conducted under environmental SEM mode (20 Pa). Samples analyzed with LEO 1530 were lightly carbon coated (50-100 Å coating). Accelerating voltages from 5 to15 kV were used.

Analyses of Mg compositions of synthetic Ca-Mg carbonates

Bulk average $MgCO_3$ content of Ca-Mg carbonates was measured based on the empirical curve (Zhang et al. 2010) correlating $MgCO_3$ contents and the shift of calcite (104) peak toward dolomite. TEM-based EDS was also used to measure $MgCO_3$ contents of typical samples (see Zhang et al. (2010) for method details).

Terminology of Ca-Mg carbonates

Ideal dolomite ($CaMg(CO_3)_2$, space group: $R\bar{3}$) has a crystal lattice consisting of alternating layers of Ca and Mg, separated by layers of CO_3, where Ca and Mg are present in equal proportions. However, very few, if any, sedimentary dolomites are truly stoichiometric $CaMg(CO_3)_2$ and are better represented as: $Ca_{(1+x)}Mg_{(1-x)}(CO_3)_2$ since most ancient dolomites are calcium-rich (Warren 2000).

Mg^{2+} incorporation into calcitic structure results in the formation of various phases, including: low-Mg calcite (space group: $R\bar{3}c$) with less than 4 mol% of $MgCO_3$, high Mg-calcite (space group: $R\bar{3}c$) with more than 4 mol% and up to 35 mol% of $MgCO_3$ according to the proposed solvus between calcite and dolomite (Anovitz and Essene 1987), disordered dolomite (with more than 35 mol% of $MgCO_3$ and typically Ca-rich with disordered cations, i.e., instead of occurring in alternating cation layers, Ca^{2+} and Mg^{2+} ions are randomly distributed; therefore, it has the same space group with calcite: $R\bar{3}c$), and dolomite (space group: $R\bar{3}$) (Zhang et al. 2012a). Dolomite with weak or partial cation ordering is often referred to as proto-dolomite, which has the same space group ($R\bar{3}$) with ideal dolomite (Goldsmith and Graf 1958; Graf and Goldsmith 1956). Proto-dolomite is generally Ca-rich (Xu, 2010).

RESULTS

During experiments with the non-metabolizing consortium biomass, shortly after NH_4HCO_3 powder and the petri dishes containing experimental solutions were put in the sealed desiccator, the decomposition of NH_4HCO_3 started and carbonate precipitation was observed between 6-8 hours as indicated by the visual cloudiness in the solution. In control solutions, precipitates also appeared between 6-8 hours. Added NH_4HCO_3 powders were completely decomposed after ~12 hours. After 14 days, the pH of the experimental solutions containing non-metabolizing consortium biomass increased from i 7.1-7.4 to 8.5-8.9 **(Table 1)**. Characterizations of carbonate precipitates sampled after 14 days clearly demonstrate that the non-metabolizing consortium biomass can catalyze the precipitation of Ca-Mg carbonates close to dolomite composition. For example, as determined by *d*-spacings of the (104) peak (d_{104}) of Ca-Mg carbonates on XRD patterns (Zhang et al. 2010), Ca-Mg carbonates with ~42 mol% of $MgCO_3$ and small amounts of aragonite were precipitated in solutions with an initial Mg:Ca ratio of 5:1 and ~820 mg/L of non-metabolizing consortium biomass **(Fig. 1b and Table 1)**. In contrast, aragonite and high-Mg calcite with only ~14 mol% of $MgCO_3$ were formed in control solutions without biomass **(Table 1 and Fig. 2b)**. When the initial Mg:Ca ratio was 8:1, a mixture of carbonates including Ca-Mg carbonates close to dolomite composition (~48 mol% $MgCO_3$), and a small amount of aragonite, monohydrocalcite ($CaCO_3 \cdot H_2O$), and nesquehonite ($MgCO_3 \cdot 3H_2O$) crystallized in solutions with consortium biomass **(Fig. 1c)**, while aragonite and high-Mg calcite with ~23 mol% of $MgCO_3$ produced in control solutions **(Fig. 2c)**. When the initial Mg:Ca ratio was 3:1, precipitates induced by non-metabolizing consortium biomass were more complicated. The major phase in the precipitates was a high-Mg calcite with ~17 mol% of $MgCO_3$, which was ~9 mol% higher than that of precipitates in control solutions **(Fig. 1a, 2a)**.

342 However, careful examination of the XRD pattern reveals the presence of an Mg-rich carbonate
343 phase as indicated by the shoulder on right of the high-Mg calcite (104) peak **(Fig. 1a and Table**
344 **1)**.

345 Experiments reveal that bound EPS was the active component in the non-metabolizing
346 biomass that promoted the precipitation of Ca-Mg carbonates close to dolomite composition. Ca-
347 Mg carbonates similar to those precipitated in solutions containing non-metabolizing consortium
348 biomass crystallized in the presence of ~177 mg/L of bound EPS extracted from ~820 mg/L of
349 biomass **(Fig. 1)**. Furthermore, the $MgCO_3$ contents in synthetic carbonates increased with bound
350 EPS concentration **(Fig. 3)**. It is also interesting to notice the products precipitated in solutions
351 containing dead cell pellets with bound EPS removed **(Fig. 4)**. For example, while high-Mg
352 calcite with ~9 mol% of $MgCO_3$ crystallized in solutions with bound EPS-removed DCP and an
353 initial Mg:Ca ratio of 3:1, the calcite precipitated at Mg:Ca ratios of 5:1 and 8:1 contained
354 negligible amounts of $MgCO_3$, even less than those from corresponding control experiments.
355 Bound EPS-removed DCP also induced the precipitation of nesquehonite and giorgiosite
356 ($Mg_5(CO_3)_4(OH)_2 \cdot 5H_2O$) **(Fig. 4)**, while the precipitates induced by bound EPS were dominated
357 by Ca-Mg carbonates close to dolomite composition, along with a small amount of
358 monohydrocalcite at high initial Mg:Ca ratios **(Fig. 4)**. Therefore, it is apparent that bound EPS
359 catalyzed the crystallization of Ca-Mg carbonates and inhibited aragonite precipitation, whereas
360 bound EPS-removed DCP induced the precipitation of hydrous Mg-carbonates.

361 To characterize the carbonate precipitation process, precipitates produced in consortium
362 bound EPS-bearing solutions were sampled at different time. Fig. 5 shows typical XRD patterns
363 of precipitated carbonates sampled at different time intervals from bound EPS-bearing solutions
364 (177 mg/L bound EPS; Mg:Ca = 5:1). A comparison between Fig. 1e and 5c shows that

365 precipitates sampled after 10 days were similar to those after 14 days, which were both Ca-Mg
366 carbonates with 44-45 mol% of $MgCO_3$. However, the peak position of precipitated carbonates
367 sampled earlier is not shifted as much to the high 2θ angle as carbonates sampled later **(compare**
368 **Fig. 5a and 5b, Fig. 5b and 5c)**. This indicates that earlier precipitates have less Mg^{2+}
369 incorporation and will evolve to Ca-Mg carbonates with higher $MgCO_3$ contents with time in the
370 presence of the EPS.

371 The abundant OTUs, as identified by 454 16S rRNA amplicon sequencing, were
372 classified as *Halanaerobium* (fermenting bacteria, comprising 47% of the total reads), *Clostridia*
373 (fermenting bacteria, comprising 25% of the total reads), *Desulfohalobiaceae* (SRB, comprising
374 13% of the total reads), and *Bacillales* (fermenting bacteria, comprising 13% of the total reads),
375 while the remaining 2% of reads were classified only as "bacteria" by RDP. The OTUs classified
376 as *Halanaerobium* were found to be a 96% match to *Halanaerobium praevalens* via BLAST.
377 OTUs classified as *Clostridia* and *Desulfohalobiaceae* were found to be 93% and 99% matches
378 to *Clostridium* sp. Gec1-52-ana4-2 and *Desulfonatronovibrio* sp.AHT21 with further BLAST
379 searching. The *Bacillales* OTUs were 99% matches to *Bacillus* sp. CG7, and the 2% of reads
380 classified only as "bacteria" via RDP were found to be a 90% match to *Clostridium* sp. Gec1-52-
381 ana4-2, indicating the possible presence of another group of *Clostridia*.

382 To determine the microorganisms in the consortium whose bound EPS was likely to have
383 promoted disordered dolomite precipitation, non-metabolizing biomass from pure cultures of
384 fermenting bacteria *H. saccharolyticum* and SRB *D. retbaense* closely related to organisms
385 present in the consortium was collected for carbonate precipitation experiments. As shown
386 above, fermenting bacteria classified as *Clostridium and Bacillales* were also abundant in the

consortium, but we focused on *H. saccharolyticum* as models. It is possible that *Clostridium* may also play an important role in dolomite formation.

Remarkably, both the non-metabolizing biomass from *H. saccharolyticum* and *D. retbaense* cultures greatly enhanced Mg^{2+} incorporation into precipitating carbonates and catalyzed the crystallization of Ca-Mg carbonates close to dolomite composition **(Fig. 6-9; Table 2)**. For instance, Ca-Mg carbonates with ~50 mol% of $MgCO_3$ crystallized in solutions with an initial Mg:Ca ratio of 5:1 and ~737 mg/L of non-metabolizing biomass of *H. saccharolyticum* **(Fig. 6c)**. In contrast, parallel controls only precipitated Ca-Mg carbonates with 12 mol% of $MgCO_3$ **(Table 2 and Fig. 8d)**. When the initial Mg:Ca ratio was 8:1, Ca-Mg carbonates induced by the non-metabolizing biomass of *H. saccharolyticum* contained as much as ~56 mol% of $MgCO_3$ **(Fig. 6d)**. Ca-Mg carbonates close to dolomite composition were also precipitated in solutions containing non-metabolizing biomass of *D. retbaense* **(Fig. 7 and 9)**. Therefore, it is likely that both the fermenting bacteria and SRB in the natural anaerobic consortium could excrete bound EPS to induce the crystallization of Ca-Mg carbonates close to dolomite composition.

SEM imaging of synthetic carbonates show that Ca-Mg carbonates close to dolomite composition grew on chalk seed crystals forming clusters with different shapes and sizes **(Fig. 10a)**. In the presence of synthetic seeds, Ca-Mg carbonates close to dolomite composition also overgrew synthetic seeds, but the rhombohedral shape of synthetic seeds was overall preserved **(Fig. 11)**. Careful observations show that Ca-Mg carbonates close to dolomite composition actually occurred as nano-crystals (~10-20 nm) **(Fig. 10b and 11d)**. TEM-based EDS confirms that the composition of Ca-Mg carbonates induced by bound EPS was close to dolomite composition **(Fig. 10b inset)**. SAED analyses show that carbonate nano-crystals were not

randomly oriented, but rather followed the orientation of seed crystals and displayed low-angle grain boundaries between neighboring nano-crystals **(Fig. 10c)**. We characterized 7 [010]-zone axis SAED and multiple fast Fourier transform patterns, none of which shows supper-lattice reflections such as (003) and ($\bar{1}$05) that would indicate Ca-Mg cation order in the dolomite structure **(see for example, Fig. 10c, d)**; thus our synthetic carbonates were fully Ca-Mg disordered.

The total polysaccharide content of the consortium bound EPS was analyzed to be 12.4±0.7 wt%, that is, ~22 mg/L out of ~177 mg/L of bound EPS. The saccharide monomer analyses show that glucose (~47 mol%), xylose (~29 mol%), and mannose (~24 mol%) are the dominant saccharide monomers of the polysaccharides in consortium bound EPS.

DISCUSSION

The mechanism by which consortium bound EPS promotes disordered dolomite precipitation deserves further discussion. The bound EPS in this study was extracted with a procedure utilizing formaldehyde and NaOH. This procedure can minimize the contamination by intracellular substances since formaldehyde could fix the cell, and thus prevent cell lysis, by reacting with the amino, hydroxyl, carboxyl and sulfhydryl function groups on the cell membrane (Liu and Fang 2002; Wingender et al. 1999). One question, however, is whether the possible reaction between bound EPS and formaldehyde played a critical role in Ca-Mg carbonate precipitation. Considering that non-metabolizing consortium biomass which was not processed with formaldehyde also catalyzed disordered dolomite precipitation, the contribution from formaldehyde should not be significant.

433 According to our data, a higher initial Mg:Ca ratio in solution results in higher $MgCO_3$
434 contents in synthetic Ca-Mg carbonates **(Fig. 3, and 9)**, which is consistent with previous
435 observations (Hardie 1987; Zhang et al. 2012b). Therefore, we may speculate that the catalytic
436 effect of bound EPS on dolomite formation was resulted from increased Mg:Ca ratio in solution
437 due to preferential binding of Ca^{2+} to bound EPS: if fewer Mg^{2+} was bound to bound EPS than
438 Ca^{2+}, the Mg:Ca ratio in solution would have sharply increased. Previous studies of the cation
439 binding capacity of soluble EPS extracted from SRB cultures yielded a Ca^{2+} binding capacity of
440 0.12-0.15 g_{Ca}/g_{EPS} (Braissant et al. 2007). Although not directly comparable, if we assume
441 preferential bound EPS binding of Ca^{2+} with 0.2 g_{Ca}/g_{EPS} and 0 g_{Mg}/g_{EPS}, the ~177 mg/L of
442 bound EPS will bind 0.885 mM Ca^{2+}, resulting in an increase in Mg:Ca ratio from 3:1, 5:1, and
443 8:1 to 3.3:1, 5.5:1, and 8.8:1, respectively. Such a small increase, which would be even smaller if
444 bound EPS also binds Mg^{2+}, obviously cannot account for the huge enhancement of Mg^{2+}
445 incorporation by bound EPS.

446 Previous studies have shown that polysaccharides can mediate calcite and disordered
447 dolomite precipitation (Bosak and Newman 2005; Braissant et al. 2003; Kawano and Hwang
448 2011; Zhang et al. 2012b). For example, Zhang et al. (2012) synthesized Mg-rich disordered
449 dolomite in solutions with ~200 mg/L of agar and an initial Mg:Ca ratio of 8:1. Kawano and
450 Hwang (2011) showed that polysaccharides can promote the precipitation of calcite while
451 inhibiting aragonite crystallization. Braissant et al. (2003) found that purified exopolysaccharides
452 (xanthan EPS) exerted a strong influence on the morphology of precipitated calcite. Based on
453 these studies, we propose polysaccharides in the bound EPS as one of the catalytic components.
454 The total polysaccharide content of the bound EPS was analyzed to be 12.4 wt%. Since as low as
455 118 mg/L of bound EPS can induce the precipitation of disordered dolomite when the initial

Mg:Ca ratio was 5:1 **(Table 1, Fig. 3)**, this suggests that as low as ~15 mg/L of polysaccharides in bound EPS may be sufficient to catalyze disordered dolomite formation. Compared to the amount of agar (200 mg/L) required to catalyze disordered dolomite crystallization, 15 mg/L of polysaccharides seems to be relatively low. However, it is noteworthy that the Mg-incorporation capacities can vary significantly among different polysaccharides. For example, disordered dolomite containing ~52 mol% of $MgCO_3$ crystallized in solutions with ~200 mg/L of agar and an initial Mg:Ca ratio of 8:1, whereas ~5 g/L of carboxymethyl cellulose was required to precipitate disordered dolomite (Zhang et al. 2012b). Another example is that several mg/L of additives such as phosphate and certain polycarboxylic acid can greatly influence the nucleation of calcium carbonate (Gallagher et al. 2013; He et al. 1999). Therefore, it is possible that as low as 15 mg/L of polysaccharides in the consortium bound EPS can catalyze disordered dolomite precipitation.

The possible existence of other catalytic components in bound EPS other than polysaccharides is also noteworthy (Braissant et al. 2003; Gautret and Trichet 2005; Raz et al. 2000; Stephenson et al. 2008; Wang et al. 2009). For example, polyacrylic and polyaspartic acids were found to be able to catalyze the crystallization of Ca-Mg carbonate with up to 34 mol% of $MgCO_3$ (Raz et al. 2000). Stephenson et al. (2008) showed that a small amount of peptides in solution can enhance the step velocity on the Ca-Mg carbonate growth hillock and slightly enhance Mg^{2+} incorporation. Along analogous lines, carboxylated organic acids with a strong affinity for binding Ca^{2+} compared to Mg^{2+} were shown to promote the formation of Mg-enriched amorphous calcium carbonates (Wang et al. 2009). These possible catalytic components, together with polysaccharides, may exert synergistic catalysis effect on the nucleation and growth of disordered dolomite.

479 Mg^{2+} incorporation into the calcitic structure has been considered as one of the most
480 critical barrier to (disordered) dolomite crystallization (Baker and Burns 1985; de Leeuw and
481 Parker 2001; Higgins and Hu 2005; Lippmann 1973; Raz et al. 2000; Xu et al. 2013). Mg^{2+},
482 which forms one of the strongest bonds with water molecules among the divalent ions (Jiao et al.
483 2006; Lippmann 1973; Noyes 1962; Raz et al. 2000; Richens 1997; Stephenson et al. 2008), may
484 only be partially dehydrated when incorporated into growing Ca-Mg carbonates. The residual
485 hydration sphere of the incorporated Mg^{2+} would then inhibit the further segregation of surface
486 Mg^{2+} ions into the bulk crystal, and thereby hinder the growth of Ca-Mg carbonates (Astilleros et
487 al. 2010; Davis et al. 2000; de Leeuw and Parker 2001; Higgins and Hu 2005; Lippmann 1973;
488 Mucci and Morse 1983; Raz et al. 2000; Stephenson et al. 2008). Similar to what we have
489 suggested in previous studies (Zhang et al. 2012a; Zhang et al. 2012b; Zhang et al. 2013), we
490 propose that the adsorption of bound EPS onto growing Ca-Mg carbonate surfaces through
491 hydrogen bonding is the key to catalyzing Mg^{2+} incorporation. The hydrogen bonding between
492 the H in the OH group of bound EPS and the O in the CO_3^{2-} on carbonate surfaces may displace
493 surface water molecules which would otherwise be associated with the hydration shell of Mg^{2+},
494 thereby facilitating Mg^{2+} incorporation and disordered dolomite crystallization. This hypothesis
495 is supported by the saccharide monomer analyses of the polysaccharides in bound EPS. Our data
496 show that glucose, xylose, and mannose were the dominant saccharide monomers of the
497 polysaccharides in bound EPS. While there is no data for glucose, molecular dynamic
498 simulations show that xylose and mannose have a stronger adsorption onto calcite (104) surfaces
499 than water (Yang et al. 2008).

500 Our experiments with non-metabolizing biomass also succeeded in precipitating
501 disordered dolomite. We suggest that bound EPS of the non-metabolizing biomass may have

been sloughed off from the cell surface into the solution during the dialysis and precipitation experiments due to the possible lysis of cells. For example, ultrasonication, which is also a common procedure used for EPS extraction (Nielsen and Jahn 1999), was used to suspend added calcite seed crystals in experimental solutions. The released bound EPS then can be adsorbed onto carbonate surfaces to promote the dehydration of surface Mg^{2+}.

IMPLICATIONS

Our synthetic dolomite is fine crystalline, Ca-rich, and cation-disordered. Similar disordered dolomite has been precipitated in laboratory experiments in SRB cultures (Bontognali et al. 2014). Interestingly, modern dolomites similar to our synthetic ones have also been widely found in natural environments where SRB are active (Bontognali et al. 2010; Van Lith et al. 2003a; Vasconcelos and McKenzie 1997; Wright 1999; Wright and Wacey 2005). For instance, fine crystalline Ca-rich disordered dolomite with a d_{104} value of 2.934 Å and high-Mg calcite with variable $MgCO_3$ contents have been found in sediments from a coastal lagoon where sulfate reduction is active (Vasconcelos and McKenzie 1997). Moreover, modern dolomites found within the zone of SRB in organic-rich continental margin sediments are also generally fine crystalline, Ca-rich and poorly ordered (Baker and Burns 1985; Compton and Siever 1984; Pisciotto and Mahoney 1981; Thornburg and Suess 1990). Ca-Mg-carbonates associated with modern deep sea methane seeps are high-magnesian calcite and poorly ordered proto-dolomite (Xu, 2010). In fact, Holocene sedimentary dolomites are commonly found to be Ca-rich and poorly cation-ordered (Bathurst 1975; Lippmann 1973). All these observations suggest that disordered dolomite may be the initially precipitated phase in these cases. With deposition,

poorly crystallized disordered dolomite may undergo maturation and recrystallization accompanied by increased cation ordering and crystallinity, which can produce partially ordered proto-dolomite and eventually, fully ordered dolomite (Gregg et al. 1992; Hardie 1987; Lippmann 1973; Vasconcelos and McKenzie 1997; Warren 2000). The cation ordering in dolomite is spontaneous according to thermodynamics; however, it is sluggish at low temperatures during sediment digenesis (Carpenter 1980; Helgeson et al. 1978). For example, dolomites from the Miocene Monterey Formation are still weakly ordered, finely crystalline and Ca-rich (Compton and Siever 1984). Partial cation order has even been found in Cambrian dolomite (Wright 1997). Therefore, time can be an important factor for the formation of sedimentary ordered dolomite (Hardie 1987). In other words, disordered dolomite induced by fermenting bacteria and SRB can be considered as a precursor to some sedimentary ordered dolomite.

In contrast, Meister et al. (2011) found that dolomite in sediments of Deep Springs Lake is ordered. It is possible that fast precipitation in our experiments resulted in the disordered structure, while the cation order in natural dolomite was caused by the slow crystallization limited by the low supersaturation level in Deeps Springs Lake (Meister et al. 2011).

This study defines a plausible role of anaerobic fermenting bacteria in sedimentary dolomite formation, which to our best knowledge has not been reported previously. Unlike SRB, which are limited to environments with high concentrations of dissolved sulfate, the ubiquitous distribution of anaerobic fermenting bacteria in both freshwater and marine environments (Jørgensen 2000) may extend the range of natural environments where microbial-induced dolomite precipitation could take place.

548

549 **ACKNOWLEDGMENTS**

550 This work was made possible by financial support from NASA Astrobiology Institute
551 (N07-5489), NSF (EAR-095800), and U.S. Department of Energy (DE-SC0001929) to H.X.; by
552 a Graduate Summer Research Grant from ExxonMobil Exploration Company and Department of
553 Geoscience, University of Wisconsin-Madison to F.Z. and Z.S.

REFERENCES CITED

Aloisi, G., Gloter, A., Kroger, M., Wallmann, K., Guyot, F., and Zuddas, P. (2006) Nucleation of calcium carbonate on bacterial nanoglobules. Geology, 34(12), 1017-1020.

Altschul, S.F., Gish, W., Miller, W., Myers, E.W., and Lipman, D.J. (1990) Basic local alignment search tool. Journal of Molecular Biology, 215(3), 403-410.

Anovitz, L.M. and Essene, E.J. (1987) Phase-equilibria in the system $CaCO_3$-$MgCO_3$-$FeCO_3$. Journal of Petrology, 28(2), 389-414.

Astilleros, J.M., Fernandez-Diaz, L., and Putnis, A. (2010) The role of magnesium in the growth of calcite: An AFM study. Chemical Geology, 271(1-2), 52-58.

Baker, P.A. and Burns, S.J. (1985) Occurrence and formation of dolomite in organic-rich continental margin sediments. AAPG Bulletin, 69(11), 1917-1930.

Bathurst, R.G.C. (1975) Carbonate Sediments and Their Diagenesis. 658 p. Elsevier, New York.

Belova, D.A., Johnsson, A., Bovet, N., Lakshtanov, L.Z., and Stipp, S.L.S. (2012) The effect on chalk recrystallization after treatment with oxidizing agents. Chemical Geology, 291, 217-223.

Benzerara, K., Menguy, N., López-García, P., Yoon, T.-H., Kazmierczak, J.z., Tyliszczak, T., Guyot, F., and Brown, G.E. (2006) Nanoscale detection of organic signatures in carbonate microbialites. Proceedings of the National Academy of Sciences USA, 103(25), 9440-9445.

Bontognali, T.R., McKenzie, J.A., Warthmann, R.J., and Vasconcelos, C. (2014) Microbially influenced formation of Mg-calcite and Ca-dolomite in the presence of exopolymeric substances produced by sulphate-reducing bacteria. Terra Nova, 26(1), 72-77.

Bontognali, T.R.R., Vasconcelos, C., Warthmann, R.J., Bernasconi, S.M., Dupraz, C., Strohmenger, C.J., and McKenzie, J.A. (2010) Dolomite formation within microbial mats in the coastal sabkha of Abu Dhabi (United Arab Emirates). Sedimentology, 57(3), 824-844.

Bontognali, T.R.R., Vasconcelos, C., Warthmann, R.J., Dupraz, C., Bernasconi, S.M., and McKenzie, J.A. (2008) Microbes produce nanobacteria-like structures, avoiding cell entombment. Geology, 36(8), 663-666.

Bosak, T. and Newman, D.K. (2005) Microbial kinetic controls on calcite morphology in supersaturated solutions. Journal of Sedimentary Research, 75(2), 190-199.

Braissant, O., Cailleau, G., Dupraz, C., and Verrecchia, A.P. (2003) Bacterially induced mineralization of calcium carbonate in terrestrial environments: The role of exopolysaccharides and amino acids. Journal of Sedimentary Research, 73(3), 485-490.

Braissant, O., Decho, A.W., Dupraz, C., Glunk, C., Przekop, K.M., and Visscher, P.T. (2007) Exopolymeric substances of sulfate-reducing bacteria: Interactions with calcium at alkaline pH and implication for formation of carbonate minerals. Geobiology, 5(4), 401-411.

Caporaso, J.G., Kuczynski, J., Stombaugh, J., Bittinger, K., Bushman, F.D., Costello, E.K., Fierer, N., Pena, A.G., Goodrich, J.K., and Gordon, J.I. (2010) QIIME allows analysis of high-throughput community sequencing data. Nature Methods, 7(5), 335-336.

Carpenter, A.B. (1980) The chemistry of dolomite formation I: The stability of dolomite. In D.H. Zenger, J.B. Dunham, and R.L. Ethington, Eds. Concepts and Models of Dolomitization, p. 111-121. Society for Sedimentary Geology, Tulsa, OK.

598 Compton, J.S. (1988) Degree of supersaturation and precipitation of organogenic dolomite.
599 Geology, 16(4), 318-321.
600 Compton, J.S. and Siever, R. (1984) Stratigraphy and dolostone occurrence in the Miocene
601 Monterey Formation, Santa Maria Basin area, California. In R.R. Garrison, M. Kastner,
602 and D.H. Zenger, Eds. Dolomites of the Monterey Formation and other organic-rich
603 units, p. 141-154. Society for Sedimentary Geology, Tulsa, OK.
604 Davis, K.J., Dove, P.M., and De Yoreo, J.J. (2000) The role of Mg^{2+} as an impurity in calcite
605 growth. Science, 290(5494), 1134-1137.
606 de Leeuw, N.H. and Parker, S.C. (2001) Surface-water interactions in the dolomite problem.
607 Physical Chemistry Chemical Physics, 3(15), 3217-3221.
608 Deng, S., Dong, H., Lv, G., Jiang, H., Yu, B., and Bischoff, M.E. (2010) Microbial dolomite
609 precipitation using sulfate reducing and halophilic bacteria: Results from Qinghai Lake,
610 Tibetan Plateau, NW China. Chemical Geology, 278(3-4), 151-159.
611 Dubois, M., Gilles, K.A., Hamilton, J.K., Rebers, P.A., and Smith, F. (1956) Colorimetric
612 method for determination of sugars and related substances. Analytical Chemistry, 28(3),
613 350-356.
614 Gallagher, K.L., Braissant, O., Kading, T.J., Dupraz, C., and Visscher, P.T. (2013) Phosphate-
615 Related Artifacts In Carbonate Mineralization Experiments. Journal of Sedimentary
616 Research, 83(1), 37-49.
617 Gautret, P., Camoin, G., Golubic, S., and Sprachta, S. (2004) Biochemical control of calcium
618 carbonate precipitation in modern lagoonal microbialites, Tikehau Atoll, French
619 Polynesia. Journal of Sedimentary Research, 74(4), 462-478.
620 Gautret, P. and Trichet, J. (2005) Automicrites in modern cyanobacterial stromatolitic deposits of
621 Rangiroa, Tuamotu Archipelago, French Polynesia: Biochemical parameters underlaying
622 their formation. Sedimentary Geology, 178(1), 55-73.
623 Goldsmith, J.R. and Graf, D.L. (1958) Relation between lattice constants and composition of the
624 Ca-Mg carbonate. American Mineralogist, 43, 84-101.
625 Graf, D.L. and Goldsmith, J.R. (1956) Some hydrothermal syntheses of dolomite and
626 protodolomite. Journal of Geology, 64, 173-186.
627 Gregg, J.M., Howard, S.A., and Mazzullo, S.J. (1992) Early diagenetic recrystallization of.
628 Holocene (< 3000 years old) peritidal dolomites, Ambergris Cay, Belize. Sedimentology,
629 39(1), 143-160.
630 Hardie, L.A. (1987) Dolomitization - a critical view of some current views. Journal of
631 Sedimentary Research, 57(1), 166-183.
632 He, S., Kan, A.T., and Tomson, M.B. (1999) Inhibition of calcium carbonate precipitation in
633 NaCl brines from 25 to 90 °C. Applied Geochemistry, 14(1), 17-25.
634 Helgeson, H.C., Delany, J.M., Nesbitt, H.W., and Bird, D.K. (1978) Summary and critique of the
635 thermodynamic properties of rock-forming minerals. American Journal of Science, 278,
636 1-229.
637 Higgins, S.R. and Hu, X.M. (2005) Self-limiting growth on dolomite: Experimental observations
638 with in situ atomic force microscopy. Geochimica et Cosmochimica Acta, 69(8), 2085-
639 2094.
640 Hsieh, K.M., Murgel, G.A., Lion, L.W., and Shuler, M.L. (1994) Interactions of microbial
641 biofilms with toxic trace metals: 1. Observation and modeling of cell growth, attachment,
642 and production of extracellular polymer. Biotechnology and Bioengineering, 44(2), 219-
643 231.

Jiao, D., King, C., Grossfield, A., Darden, T.A., and Ren, P.Y. (2006) Simulation of Ca^{2+} and Mg^{2+} solvation using polarizable atomic multipole potential. Journal of Physical Chemistry B, 110(37), 18553-18559.

Jones, B.F. (1965) The hydrology and mineralogy of Deep Springs Lake, Inyo County, California. Closed-Basin Investigations: US Geological Survey Professional Paper 502-A, A1-A56.

Jørgensen, B.B. (2000) Bacteria and Marine Biogeochimistry. In H.D. Schulz, and M. Zabel, Eds. Marine Geochemistry, p. 173-207. Springer, Berlin.

Kawaguchi, T. and Decho, A.W. (2002) A laboratory investigation of cyanobacterial extracellular polymeric secretions (EPS) in influencing $CaCO_3$ polymorphism. Journal of Crystal Growth, 240(1), 230-235.

Kawano, M. and Hwang, J. (2011) Roles of microbial acidic polysaccharides in precipitation rate and polymorph of calcium carbonate minerals. Applied Clay Science, 51(4), 484-490.

Kenward, P.A., Goldstein, R.H., Gonzalez, L.A., and Roberts, J.A. (2009) Precipitation of low-temperature dolomite from an anaerobic microbial consortium: the role of methanogenic Archaea. Geobiology, 7(5), 556-565.

Land, L.S. (1998) Failure to precipitate dolomite at 25 ^{o}C from dilute solution despite 1000-fold oversaturation after 32 years. Aquatic Geochemistry, 4(3-4), 361-368.

Laspidou, C.S. and Rittmann, B.E. (2002) A unified theory for extracellular polymeric substances, soluble microbial products, and active and inert biomass. Water Research, 36(11), 2711-2720.

Lippmann, F. (1973) Sedimentary Carbonate Minerals. 228 p. Springer, New York.

Liu, H. and Fang, H.H.P. (2002) Extraction of extracellular polymeric substances (EPS) of sludges. Journal of Biotechnology, 95(3), 249-256.

Liu, Z.Z., Lozupone, C., Hamady, M., Bushman, F.D., and Knight, R. (2007) Short pyrosequencing reads suffice for accurate microbial community analysis. Nucleic Acids Research, 35(18).

Machel, H.G. and Mountjoy, E.W. (1986) Concepts and models of dolomitization: a critical reappraise. Earth-Science Reviews, 23(3), 175-222.

Mazzullo, S.J. (2000) Organogenic dolomitization in peritidal to deep-sea sediments. Journal of Sedimentary Research, 70(1), 10-23.

Meister, P., Reyes, C., Beaumont, W., Rincon, M., Collins, L., Berelson, W., Stott, L., Corsetti, F., and Nealson, K.H. (2011) Calcium and magnesium-limited dolomite precipitation at Deep Springs Lake, California. Sedimentology, 58(7), 1810-1830.

Merkle, R.K. and Poppe, I. (1994) Carbohydrate composition analysis of glycoconjugates by gas-liquid chromatography/mass spectrometry. Methods in Enzymology, 230, 1-15.

Mucci, A. and Morse, J.W. (1983) The incorporation of Mg^{2+} and Sr^{2+} into calcite overgrowths - Influences of growth-rate and solution composition. Geochimica et Cosmochimica Acta, 47(2), 217-233.

Nielsen, P.H. and Jahn, A. (1999) Extraction of EPS. In J. Wingender, T.R. Neu, and H.-C. Flemming, Eds. Microbial Extracellular Polymeric Substances, p. 49-72. Springer, Berlin.

Nielsen, P.H., Jahn, A., and Palmgren, R. (1997) Conceptual model for production and composition of exopolymers in biofilms. Water Science and Technology, 36(1), 11-19.

Noyes, R.M. (1962) Thermodynamics of ion hydration as a measure of effective dielectric properties of water. Journal of American Chemical Society, 84(4), 513-522.

690 Ollivier, B., Hatchikian, C.E., Prensier, G., Guezennec, J., and Garcia, J.L. (1991)
691 *Desulfohalobium retbaense* gen. nov., sp. nov., a halophilic sulfate-reducing bacterium
692 from sediments of a hypersaline lake in Senegal. International Journal of Systematic
693 Bacteriology, 41(1), 74-81.
694 Pakulski, J.D. and Benner, R. (1992) An improved method for the hydrolysis and MBTH
695 analysis of dissolved and particulate carbohydrates in seawater. Marine Chemistry, 40(3-
696 4), 143-160.
697 Parkhurst, D.L. and Appelo, C.A.J. (1999) User's guide to PHREEQC (Version 2)–A computer
698 program for speciation, batch-reaction, one-dimensional transport, and inverse
699 geochemical calculations. US Geological Survey, Denver, CO.
700 Pisciotto, K.A. and Mahoney, J.J. (1981) Isotopic survey of diagenetic carbonates, Deep Sea
701 Drilling Project Leg 63. Initial Report of Deep Sea Drilling Project, 63, 595-609.
702 Rainey, F.A., Zhilina, T.N., Boulygina, E.S., Stackebrandt, E., Tourova, T.P., and Zavarzin, G.A.
703 (1995) The taxonomic status of the fermentative halophilic anaerobic bacteria:
704 Description of *Haloanaerobiales* ord. nov., *Halobacteroidaceae* fam. nov., *Orenia* gen.
705 nov. and further taxonomic rearrangements at the genus and species level. Anaerobe,
706 1(4), 185-199.
707 Raz, S., Weiner, S., and Addadi, L. (2000) Formation of high-magnesian calcites via an
708 amorphous precursor phase: Possible biological implications. Advanced Materials, 12(1),
709 38-42.
710 Richens, D.T. (1997) The Chemistry of Aqua Ions. John Wiley & Sons, Chichester, UK.
711 Roberts, J.A., Bennett, P.C., Gonzalez, L.A., Macpherson, G.L., and Milliken, K.L. (2004)
712 Microbial precipitation of dolomite in methanogenic groundwater. Geology, 32(4), 277-
713 280.
714 Stephenson, A.E., DeYoreo, J.J., Wu, L., Wu, K.J., Hoyer, J., and Dove, P.M. (2008) Peptides
715 enhance magnesium signature in calcite: Insights into origins of vital effects. Science,
716 322(5902), 724-727.
717 Thornburg, T.M. and Suess, E. (1990) Carbonate cementation of granular and fracture porosity:
718 Implications for the Cenozoic hydrologic development of the Peru continental margin.
719 Proceedings of Ocean Drilling Project, Scientific Results, 112, 95-109.
720 Van Lith, Y., Warthmann, R., Vasconcelos, C., and McKenzie, J.A. (2003a) Microbial
721 fossilization in carbonate sediments: a result of the bacterial surface involvement in
722 dolomite precipitation. Sedimentology, 50(2), 237-245.
723 -. (2003b) Sulphate-reducing bacteria induce low-temperature Ca-dolomite and high Mg-calcite
724 formation. Geobiology, 1(1), 71-79.
725 Vasconcelos, C. and McKenzie, J.A. (1997) Microbial mediation of modern dolomite
726 precipitation and diagenesis under anoxic conditions (Lagoa Vermelha, Rio de Janeiro,
727 Brazil). Journal of Sedimentary Research, 67(3), 378-390.
728 Vasconcelos, C., McKenzie, J.A., Bernasconi, S., Grujic, D., and Tien, A.J. (1995) Microbial
729 mediation as a possible mechanism for natural dolomite formation at low-temperatures.
730 Nature, 377(6546), 220-222.
731 Wang, D., Wallace, A.F., De Yoreo, J.J., and Dove, P.M. (2009) Carboxylated molecules
732 regulate magnesium content of amorphous calcium carbonates during calcification.
733 Proceedings of the National Academy of Sciences USA, 106(51), 21511-21516.

734 Wang, Q., Garrity, G.M., Tiedje, J.M., and Cole, J.R. (2007) Naïve Bayesianclassifier for rapid
735 assignment of rRNA sequences into the new bacterial taxonomy. Applied and
736 Environmental Microbiology, 73(16), 5261-5267.
737 Warren, J. (2000) Dolomite: occurrence, evolution and economically important associations.
738 Earth-Science Reviews, 52(1-3), 1-81.
739 Warthmann, R., van Lith, Y., Vasconcelos, C., McKenzie, J.A., and Karpoff, A.M. (2000)
740 Bacterially induced dolomite precipitation in anoxic culture experiments. Geology,
741 28(12), 1091-1094.
742 Whitman, W.B., Ankwanda, E., and Wolfe, R.S. (1982) Nutrition and carbon metabolism of
743 *Methanococcus voltae*. Journal of Bacteriology, 149(3), 852-863.
744 Wingender, J., Neu, T.R., and Flemming, H.-C. (1999) Microbial extracellular polymeric
745 substances: characterization, structure, and function. 258 p. Springer, Berlin.
746 Wolin, E.A., Wolin, M.J., and Wolfe, R.S. (1963) Formation of methane by bacterial extracts.
747 Journal of Biological Chemistry, 238, 2882-2886.
748 Wright, D.T. (1997) An organogenic origin for widespread dolomite in the Cambrian Eilean
749 Dubh Formation, northwestern Scotland. Journal of Sedimentary Research, 67(1), 54-64.
750 -. (1999) The role of sulphate-reducing bacteria and cyanobacteria in dolomite formation in distal
751 ephemeral lakes of the Coorong region, South Australia. Sedimentary Geology, 126(1-4),
752 147-157.
753 Wright, D.T. and Wacey, D. (2005) Precipitation of dolomite using sulphate-reducing bacteria
754 from the Coorong Region, South Australia: significance and implications.
755 Sedimentology, 52(5), 987-1008.
756 Xu, H. (2010) Synergistic roles of microorganisms in mineral precipitates associated with deep
757 sea methane seeps. In Larry L. Barton, Martin Mandl and Alexander Loy (Editors)
758 Geomicrobiology: Molecular and Environmental Perspective, p. 325-346. Springer.
759 Xu, J., Yan, C., Zhang, F., Konishi, H., Xu, H., and Teng, H.H. (2013) Testing the cation-
760 hydration effect on the crystallization of Ca-Mg-CO_3 systems. Proceedings of the
761 National Academy of Sciences USA, 110(44), 17750-17755.
762 Yang, M.J., Stipp, S.L.S., and Harding, J. (2008) Biological control on calcite crystallization by
763 polysaccharides. Crystal Growth & Design, 8(11), 4066-4074.
764 York, W.S., Darvill, A.G., McNeil, M., Stevenson, T.T., and Albersheim, P. (1986) Isolation and
765 characterization of plant cell walls and cell wall components. Methods in Enzymology,
766 118, 3-40.
767 Zenger, D.H., Dunham, J.B., and Ethington, R.L. (1980) Concepts and Models of
768 Dolomitization. 320 p. Society for Sedimentary Geology, Tulsa, OK.
769 Zhang, F., Xu, H., Konishi, H., Kemp, J.M., Roden, E.E., and Shen, Z. (2012a) Dissolved
770 sulfide-catalyzed precipitation of disordered dolomite: Implications for the formation
771 mechanism of sedimentary dolomite. Geochimica et Cosmochimica Acta, 97, 148-165.
772 Zhang, F., Xu, H., Konishi, H., and Roden, E.E. (2010) A relationship between d_{104} value and
773 composition in the calcite - disordered dolomite solid solution series. American
774 Mineralogist, 95(11-12), 1650-1656.
775 Zhang, F., Xu, H., Konishi, H., Shelobolina, E.S., and Roden, E.E. (2012b) Polysaccharide-
776 catalyzed nucleation and growth of disordered dolomite: A potential precursor of
777 sedimentary dolomite. American Mineralogist, 97(4), 556-567.

778 Zhang, F., Yan, C., Teng, H.H., Roden, E.E., and Xu, H. (2013) *In situ* AFM observations of
779 Ca–Mg carbonate crystallization catalyzed by dissolved sulfide: Implications for
780 sedimentary dolomite formation. Geochimica et Cosmochimica Acta, 105, 44-55.
781 Zhilina, T.N., Zavarzin, G.A., Bulygina, E.S., Kevbrin, V.V., Osipov, G.A., and Chumakov,
782 K.M. (1992) Ecology, physiology and taxonomy studies on a new taxon of
783 *Haloanaerobiaceae*, *Haloincola saccharolytica* gen. nov., sp. nov. Systematic and
784 Applied Microbiology, 15(2), 275-284.
785 Zhilina, T.N., Zavarzin, G.A., Rainey, F.A., Pikuta, E.N., Osipov, G.A., and Kostrikina, N.A.
786 (1997) *Desulfonatronovibrio hydyogenovorans* gen. nov., sp. nov., an alkaliphilic,
787 sulfate-reducing bacterium. International Journal of Systematic Microbiology, 47(1),
788 144-149.
789

790 **Table 1.** Chemical conditions employed in carbonate precipitation experiments with non-metabolizing consortium biomass, bound
791 EPS of consortium, and DCP with bound EPS removed and compositions of synthetic carbonates. Errors represent standard deviation.
792
793

Experiments	Initial Ca^{2+} (mM)	Initial Mg^{2+} (mM)	Initial pH	Final pH*	Final Ca^{2+} (mM)*	Final Mg^{2+} (mM)*	$MgCO_3$ content based on d_{104} (mol%)†
Control	10.1±0.2	30.3±0.2	7.7	9.0	0.28±0.05	29.6±0.2	7.4±0.8
	10.1±0.2	53.9±0.6	7.8	8.9	0.23±0.06	53.0±0.4	13.8±0.9
	10.1±0.2	79.3±0.5	7.8	9.0	0.54±0.05	77.7+0.4	23±1
Non-Metabolizing	10.2±0.2	31.1±0.9	7.1	8.9	0.21±0.01	24.6±0.7	17±3 and 52±3
Consortium Biomass	10.2±0.2	51.3±0.7	7.3	8.7	0.21±0.02	44.7±0.5	42±1
(820±8 mg/L)	10.2±0.2	80±1.1	7.4	8.5	0.29±0.03	71.4±0.6	47.5±0.9
Bound EPS of Consortium (mg/L)							
177±2	10.2±0.4	30.1±0.3	7.2	9.0	0.17±0.06	23.3±0.6	23±3 and 54±2
58.9±0.7	10.2±0.4	53.6±0.5	7.7	9.0	0.15±0.05	50.7±0.5	19±3
118±1	10.2±0.4	53.5±0.5	7.5	9.0	0.17±0.06	47.2±0.4	42.8±0.4
177±2	10.2±0.4	54.2±0.9	7.4	8.8	0.14±0.05	45.5±0.2	45.0±0.4
58.9±0.7	10.2±0.4	78.9±0.5	7.8	9.0	0.32±0.06	73.8±0.2	37±2
118±1	10.2±0.4	80.9±0.8	7.6	9.0	0.34±0.06	73.2±0.6	44±2
177±2	10.2±0.4	81±1.2	7.4	8.8	0.24±0.06	73.2+0.4	47.7±0.6
DCP of Consortium with	9.9±0.2	30.6±0.6	7.6	9.0	0.13±0.02	28.2±0.7	9±1
Bound EPS Removed	9.9±0.2	54±1	7.8	8.7	0.16±0.02	48.3±1.4	<1†
(660±5 mg/L)	9.9±0.2	81.9±0.8	7.9	8.7	0.44±0.05	75.8±0.4	<1†

*pH, Ca^{2+} and Mg^{2+} concentrations measured 14 days after carbonate precipitation experiments started.
†Molar content of $MgCO_3$ in synthetic Ca-Mg carbonates based on the empirical curve (Zhang et al., 2010) correlating the $MgCO_3$ content and the shift of carbonate (104) peak toward dolomite.
‡The (104) peaks in these products almost overlap with that of chalk seeds, indicating very small amounts of Mg^{2+} incorporation.

794 **Table 2.** Chemical conditions employed in carbonate precipitation experiments with the *H. saccharolyticum* and *D. retbaense* non-
795 metabolizing biomass and compositions of synthetic carbonates. Errors represent standard deviation.

796
797

Experiments	Initial Ca^{2+} (mM)	Initial Mg^{2+} (mM)	Initial pH	Final pH*	Final Ca^{2+} (mM)*	Final Mg^{2+} (mM)*	$MgCO_3$ content based on d_{104} (mol%)
Control	5.2±0.2	9.7±0.2	7.8	9.3	0.05±0.02	9.41±0.08	5.0±0.8
	5.2±0.2	15.0±0.2	7.8	9.3	0.05±0.01	14.6±0.2	7±1
	5.2±0.2	20.6±0.3	7.8	9.2	0.09±0.03	20.1±0.3	9.1±0.8
	5.2±0.2	24.8±0.1	7.8	9.2	0.14±0.01	24.2±0.2	11.9±0.7
	5.2±0.2	40.5±0.3	7.9	9.2	0.19±0.01	39.5±0.3	18±1
H. saccharolyticum Biomass (737±14 mg/L)	4.9±0.2	9.6±0.1	7.0	9.1	0.09±0.03	8.1±0.2	22.8±0.8
	4.9±0.2	14.7±0.1	6.9	9.0	0.20±0.05	12.8±0.3	32.0±0.1
	4.9±0.2	25.2±0.3	6.9	9.0	0.33±0.07	20.9±0.2	50±1
	4.9±0.2	41.1±0.4	7.0	9.0	0.71±0.02	36.6±0.2	56.3±0.9
D. retbaense Biomass (667±20 mg/L)	5.1±0.1	15.2±0.1	7.3	9.2	0.34±0.02	13.9 ±0.2	24.3±0.4
	5.1±0.1	21.0±0.4	7.3	9.1	0.42±0.02	18.9±0.3	33±4
	5.1±0.1	26.2±0.5	7.3	9.0	0.47±0.01	23.1±0.3	40.9±0.5
	5.1±0.1	42.0±0.5	7.4	9.0	0.51±0.03	38.6±0.5	46±1

*pH, Ca^{2+} and Mg^{2+} concentrations measured 14 days after carbonate precipitation experiments started.
†Molar content of $MgCO_3$ in synthetic Ca-Mg carbonates based on the empirical curve (Zhang et al., 2010) correlating the $MgCO_3$ content and the shift of carbonate (104) peak toward dolomite.

798 **FIGURE 1.** Typical XRD patterns of synthetic carbonates induced by non-metabolizing
799 consortium biomass and bound EPS. Peaks correspond to: A: aragonite; C: chalk seeds; D: Ca-
800 Mg carbonates close to dolomite composition; M: monohydrocalcite; N: nesquehonite.
801 (a): With an initial Mg:Ca ration of 3:1 in experimental solutions containing non-metabolizing
802 consortium biomass, high-Mg calcite with 17.5 mol% $MgCO_3$ (d_{104} = 2.9851 Å) was the major
803 phase in the precipitates, but the shoulder (pointed by the red arrow) on the calcite (104) peak
804 indicates that a Ca-Mg carbonate phase close to dolomite composition also precipitated.
805 (b): Ca-Mg carbonates close to dolomite composition (d_{104} = 2.9379 Å, 42.3 mol% of $MgCO_3$)
806 precipitated in consortium biomass-bearing solutions (Mg:Ca = 5:1). Aragonite was also present
807 in the precipitates.
808 (c): Ca-Mg carbonates close to dolomite composition (d_{104} = 2.9283 Å, 48.0 mol% of $MgCO_3$)
809 precipitated in non-metabolizing consortium biomass-bearing solutions (Mg:Ca = 8:1).
810 Aragonite, monohydrocalcite and nesquehonite were also present in the precipitates.
811 (d): With an initial Mg:Ca ration of 3:1 in experimental solutions containing bound EPS (177±6
812 mg/L), high-Mg calcite with 20.4 mol% $MgCO_3$ (d_{104} = 2.9783 Å) was the major phase in the
813 precipitates, but the shoulder (pointed by the red arrow) indicates a Mg-rich carbonate phase as
814 in (a).
815 (e): Ca-Mg carbonates close to dolomite composition (d_{104} = 2.9326 Å, 45.3 mol% of $MgCO_3$)
816 precipitated in bound EPS-bearing solutions (177 mg/L, Mg:Ca = 5:1). Monohydrocalcite was
817 also present in the precipitates.
818 (f): Ca-Mg carbonates close to dolomite composition (d_{104} = 2.9291 Å, 47.2 mol% of $MgCO_3$)
819 precipitated in bound EPS-bearing solutions (177 mg/L, Mg:Ca = 8:1). Monohydrocalcite was
820 also present in the precipitates.

821

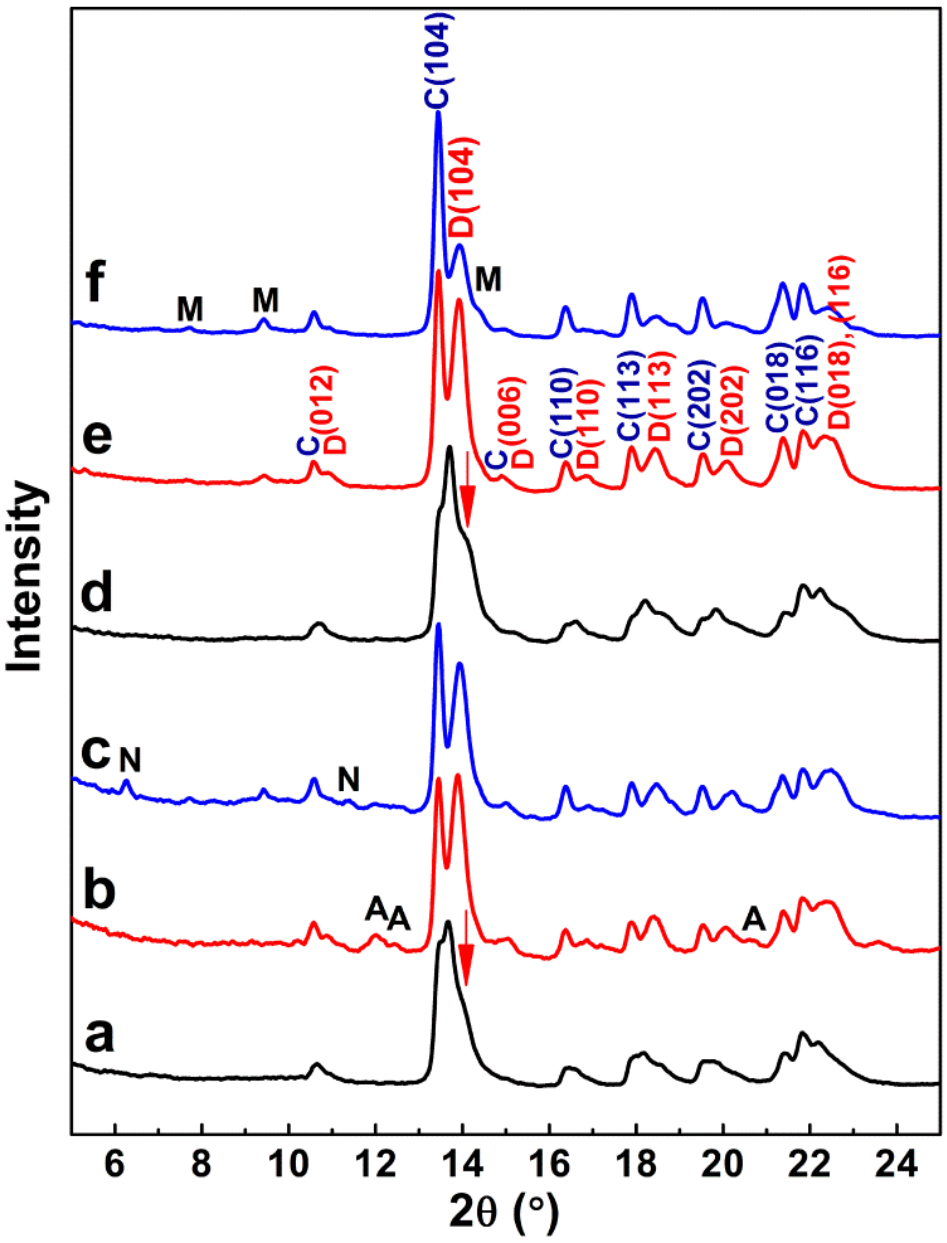

822

FIGURE 2. Typical XRD patterns of synthetic carbonates from control experiments with chalk seeds. The initial Mg:Ca ratio of the solutions in which carbonates precipitated was 3:1 (a), 5:1 (b), and 8:1 (c), respectively. Peaks correspond to: A: aragonite; C: chalk seeds; H: high-Mg calcite.

(a): High-Mg calcite (d_{104} = 3.0125 Å, 8.5 mol% $MgCO_3$).

(b): Aragonite and high-Mg calcite (d_{104} = 2.9962 Å, 13.7 mol% $MgCO_3$).

(c): Aragonite and high-Mg calcite (d_{104} = 2.9720 Å, 22.5 mol% $MgCO_3$).

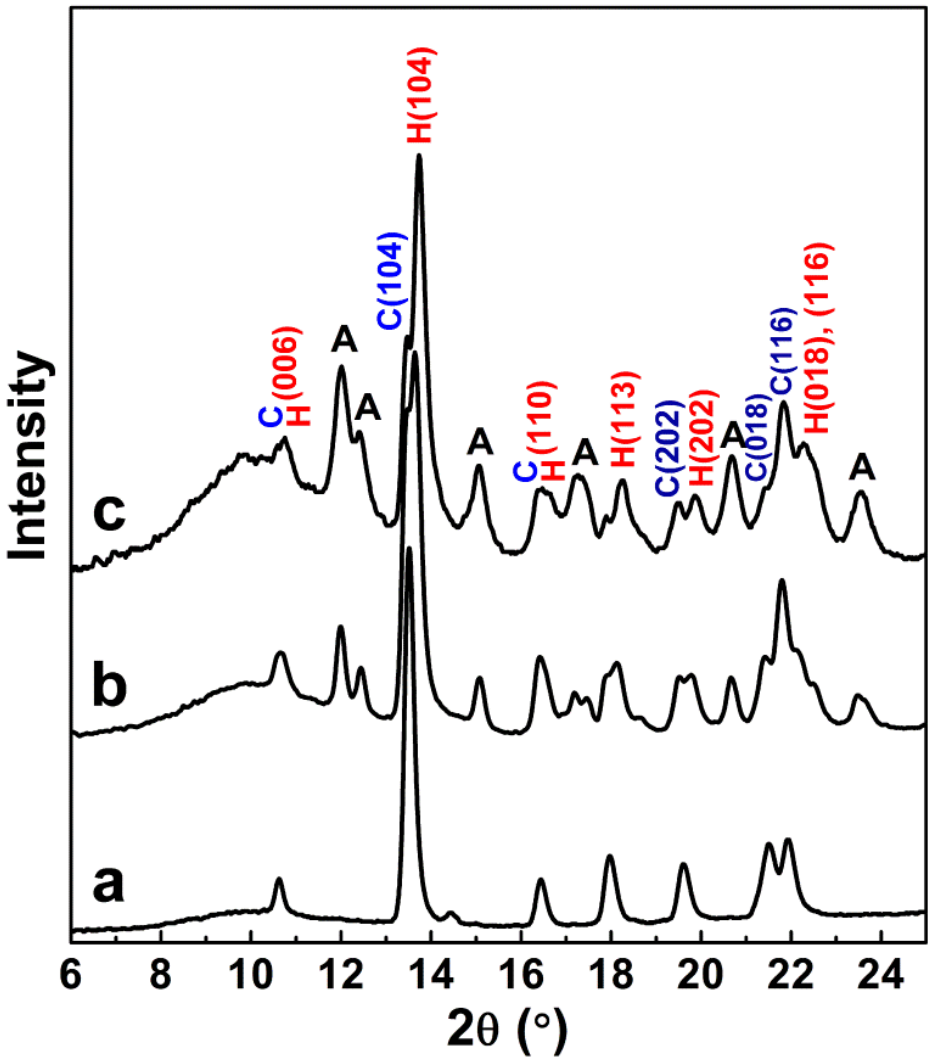

832 **FIGURE 3.** The variation of $MgCO_3$ content in synthetic Ca-Mg carbonates as a function of
833 consortium bound EPS concentration and initial Mg:Ca ratio in the solution. $MgCO_3$ content in
834 synthetic carbonates was determined based on the empirical curve (Zhang et al., 2010)
835 correlating the $MgCO_3$ content and the shift of carbonate (104) peak toward dolomite (see Table
836 1). Error bars represent standard deviation of at least duplicate samples.

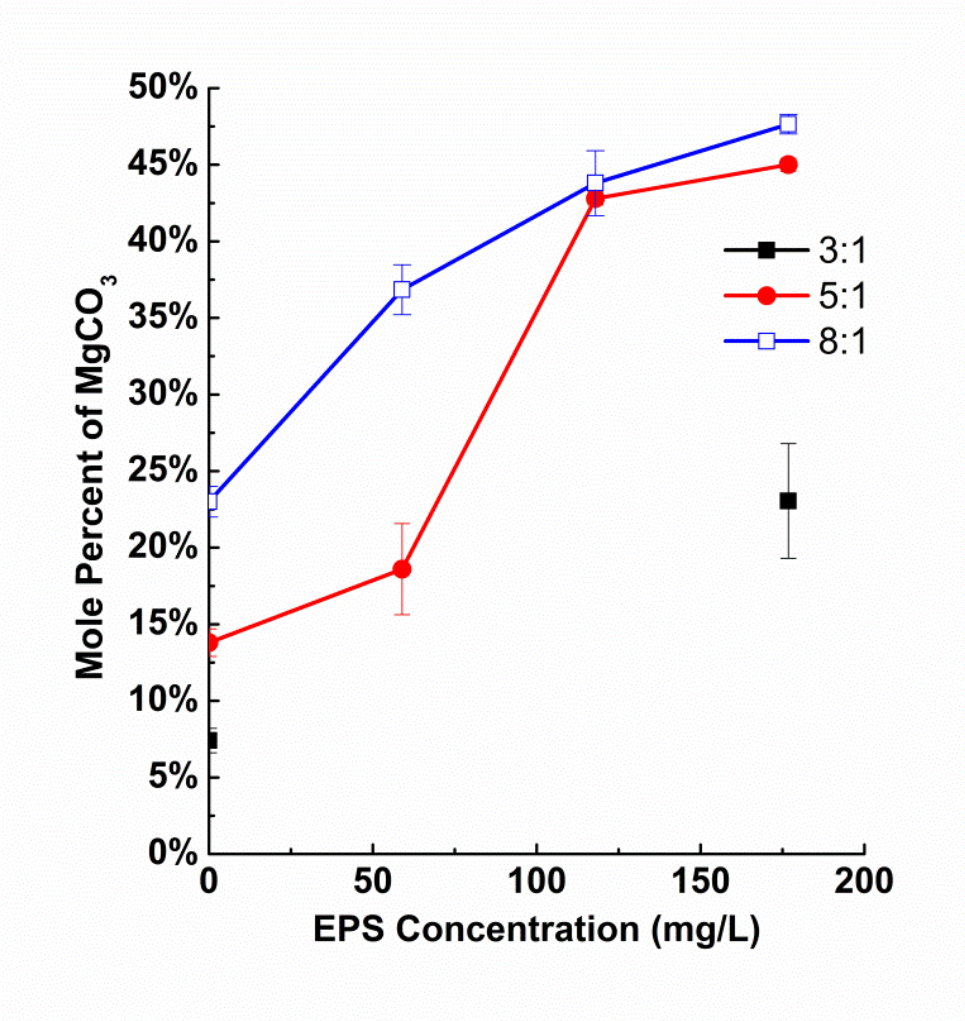

837

838 **FIGURE 4.** Typical XRD patterns of synthetic carbonates induced by DCP with bound EPS
839 removed. Peaks correspond to: A: aragonite, C: chalk seeds or low-Mg calcite, G: giorgiosite, N:
840 nesquehonite. The initial Mg:Ca ratio was 3:1 (a), 5:1 (b), and 8:1 (c), respectively. Aragonite,
841 giorgiosite, and nesquehonite are the major phases in the precipitates. The calcite (104) peak in
842 (a) is at 3.010 Å, indicating the precipitation of a Mg-calcite phase (8.9 mol% $MgCO_3$). The
843 (104) peaks in (b) and (c) almost overlap with that of chalk seeds, indicating very small amounts
844 of Mg^{2+} incorporation.

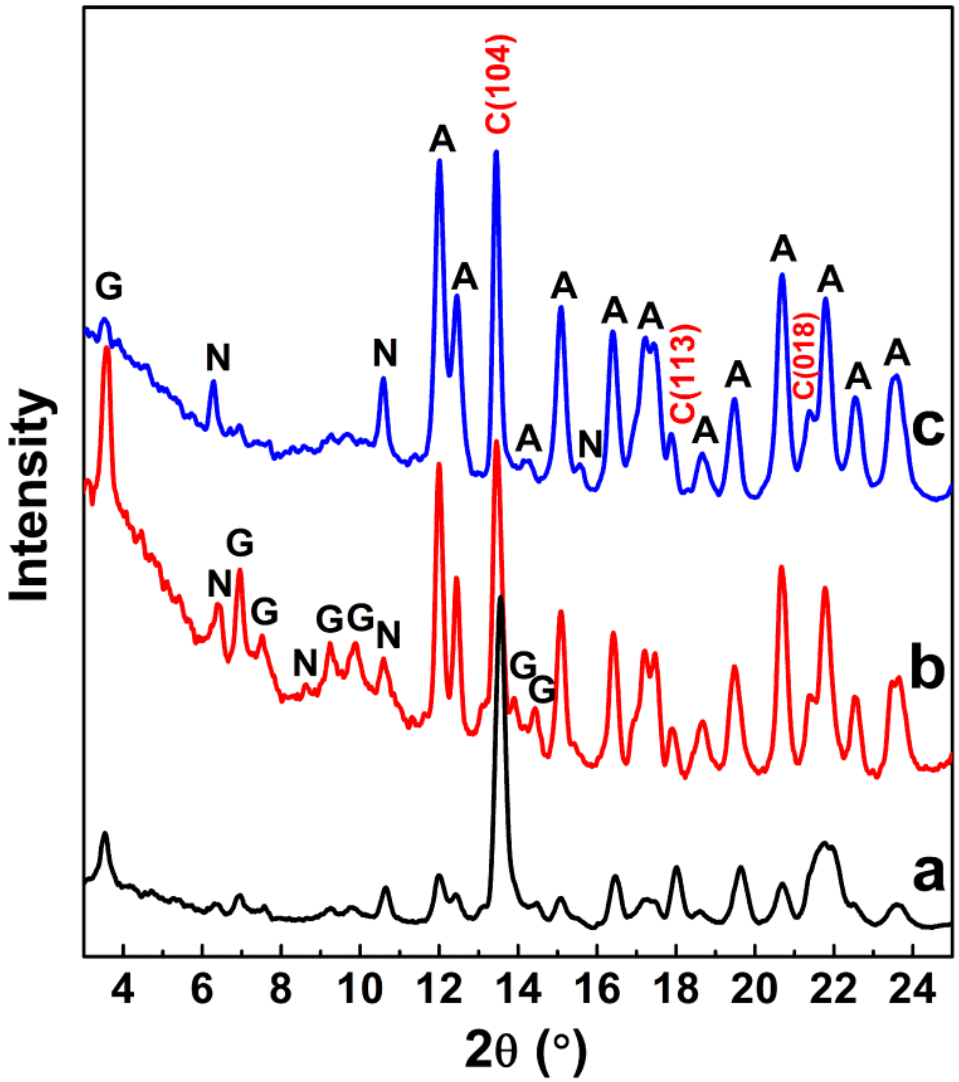

845

FIGURE 5. XRD patterns of synthetic carbonates sampled at different time from consortium bound EPS-bearing solutions (177 mg/L bound EPS; Mg:Ca = 5:1). Peaks correspond to: C: chalk seeds; D: Ca-Mg carbonate close to dolomite composition.

(a) and (b): Precipitates sampled 3 and 7 days after experiment started, respectively. The shoulder (pointed by the red arrow) on the chalk seed (104) peak indicates the (104) peak of precipitated Ca-Mg carbonates. The shift of (104) peak to high 2θ angle is more in (b) than in (a) indicating higher $MgCO_3$ content in the precipitates sampled after 7 days compared to those sampled after 3 days.

(c): Precipitates sampled 10 days after experiment started. The shift of (104) peak to high 2θ angle is more in (c) than in (b), indicating more Mg^{2+} incorporation into precipitates from day 7 to 10. Ca-Mg carbonates sampled after 10 days contained 44.1 mol% of $MgCO_3$, which was quite close to the final products sampled after 14 days **(Fig. 1e)**.

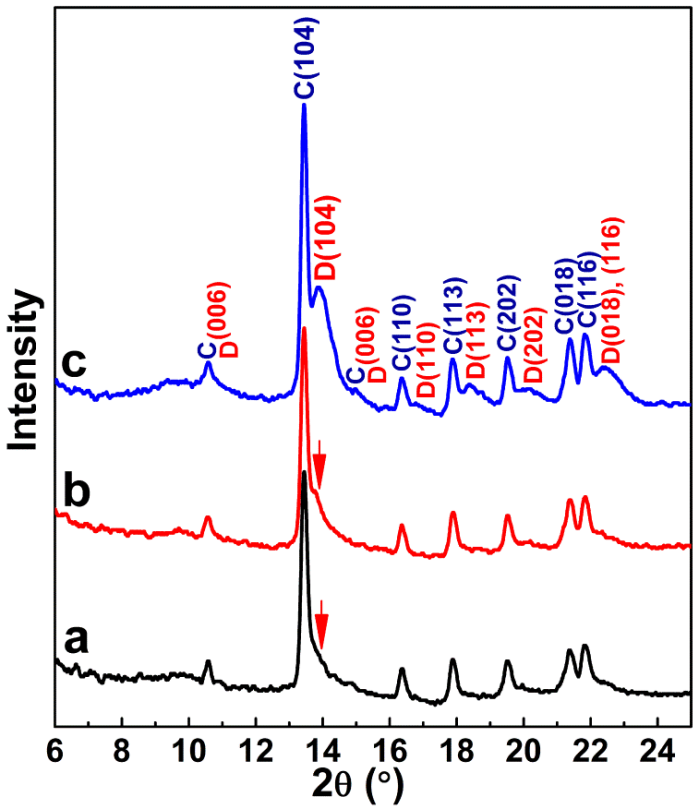

FIGURE 6. Typical XRD patterns of synthetic Ca-Mg carbonates induced by non-metabolizing *H. saccharolyticum* biomass (737±14 mg/L). The initial Mg:Ca ratio of the solutions in which carbonates precipitated was 2:1 (a), 3:1 (b), 5:1 (c), and 8:1 (d), respectively. Peaks correspond to: A: aragonite; C: synthetic seeds; D: Ca-Mg carbonates close to dolomite composition; H: high-Mg calcite; M: monohydrocalcite.

(a): High-Mg calcite (d_{104} = 2.9703 Å, 23.4 mol% of $MgCO_3$) and aragonite.

(b): High-Mg calcite (d_{104} = 2.9532 Å, 32.0 mol% of $MgCO_3$) and aragonite.

(c): Ca-Mg carbonate close to dolomite composition (d_{104} = 2.9245 Å, 50.1 mol% of $MgCO_3$) and monohydrocalcite.

(d): Mg-rich carbonate (d_{104} = 2.9108 Å, 56.9 mol% of $MgCO_3$).

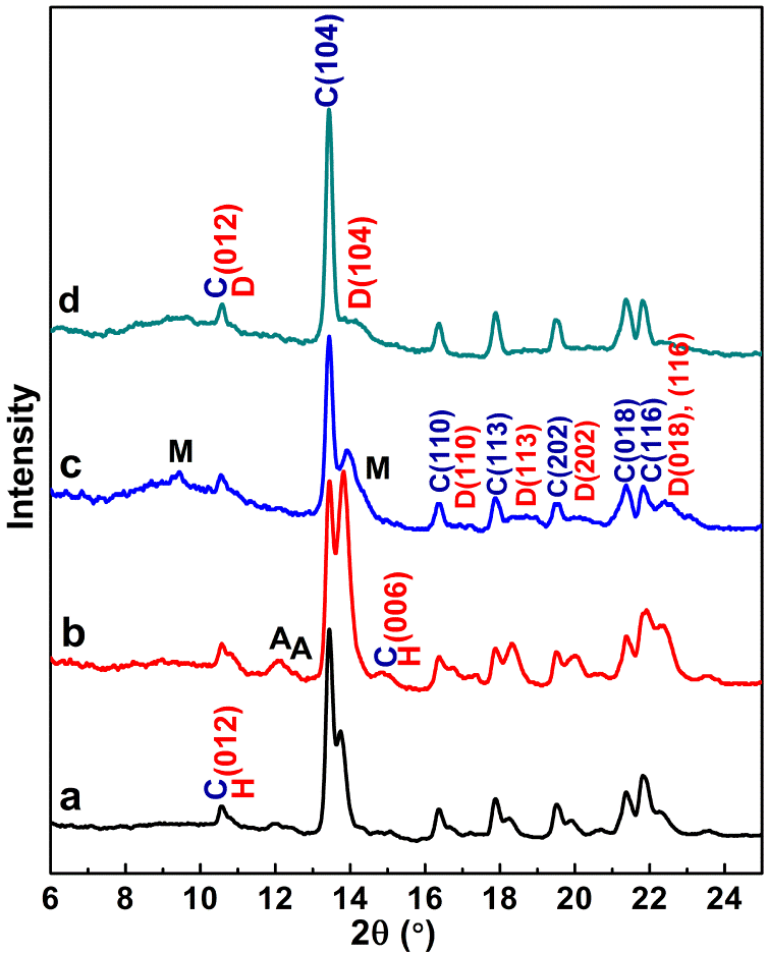

FIGURE 7. Typical XRD patterns of synthetic Ca-Mg carbonates induced by non-metabolizing *D. retbaense* biomass (667±21 mg/L). The initial Mg:Ca ratio of the solutions in which carbonates precipitated was 3:1 (a), 4:1 (b), 5:1 (c), and 8:1 (d), respectively. Peaks correspond to: A: aragonite; C: synthetic seeds; D: Ca-Mg carbonates close to dolomite composition; H: high-Mg calcite; M: monohydrocalcite.

(a): High-Mg calcite (d_{104} = 2.9677 Å, 24.5 mol% of $MgCO_3$) and aragonite.

(b): High-Mg calcite (d_{104} = 2.9561 Å, 30.4 mol% of $MgCO_3$) and aragonite.

(c): Ca-Mg carbonate close to dolomite composition (d_{104} = 2.9420 Å, 40.5 mol% of $MgCO_3$) and monohydrocalcite.

(d): Ca-Mg carbonate close to dolomite composition (d_{104} = 2.9320 Å, 45.5 mol% of $MgCO_3$) and monohydrocalcite.

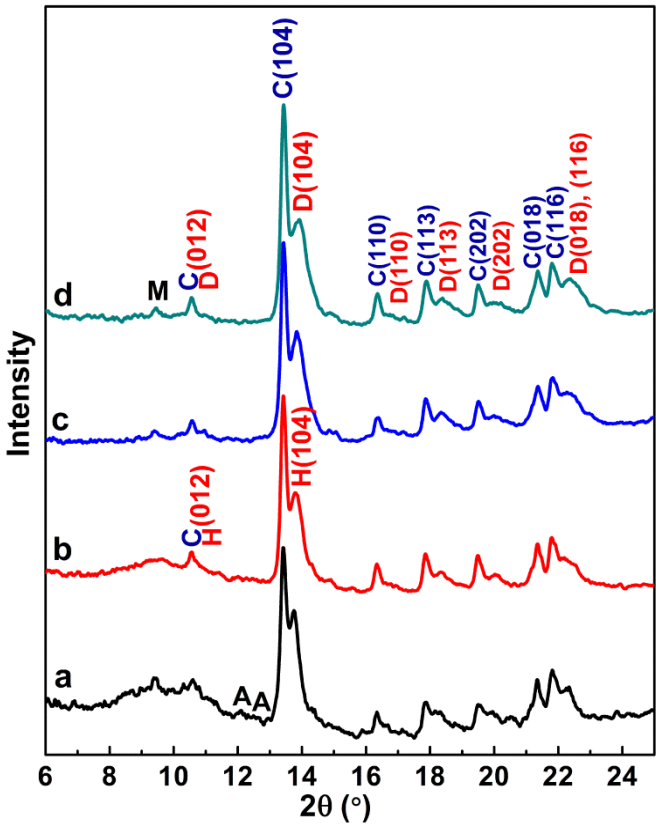

883 **FIGURE 8.** XRD patterns of synthetic high-Mg calcite from control experiments with synthetic
884 calcite seeds. The initial Mg:Ca ratio of the solutions in which carbonates precipitated was 2:1
885 (a), 3:1 (b), 4:1 (c), 5:1 (d), and 8:1 (e), respectively. Peaks correspond to: A: aragonite; C:
886 synthetic calcite seeds; H: high-Mg calcite.

887 (a): Aragonite and high-Mg calcite (d_{104} = 3.0202 Å, 5.4 mol% $MgCO_3$).

888 (b): Aragonite and high-Mg calcite (d_{104} = 3.0128 Å, 8.4 mol% $MgCO_3$).

889 (c): Aragonite and high-Mg calcite (d_{104} = 3.0078 Å, 9.5 mol% $MgCO_3$).

890 (d): Aragonite and high-Mg calcite (d_{104} = 3.0027 Å, 11.5 mol% $MgCO_3$).

891 (e): Aragonite and high-Mg calcite (d_{104} = 2.9831 Å, 18.5 mol% $MgCO_3$).

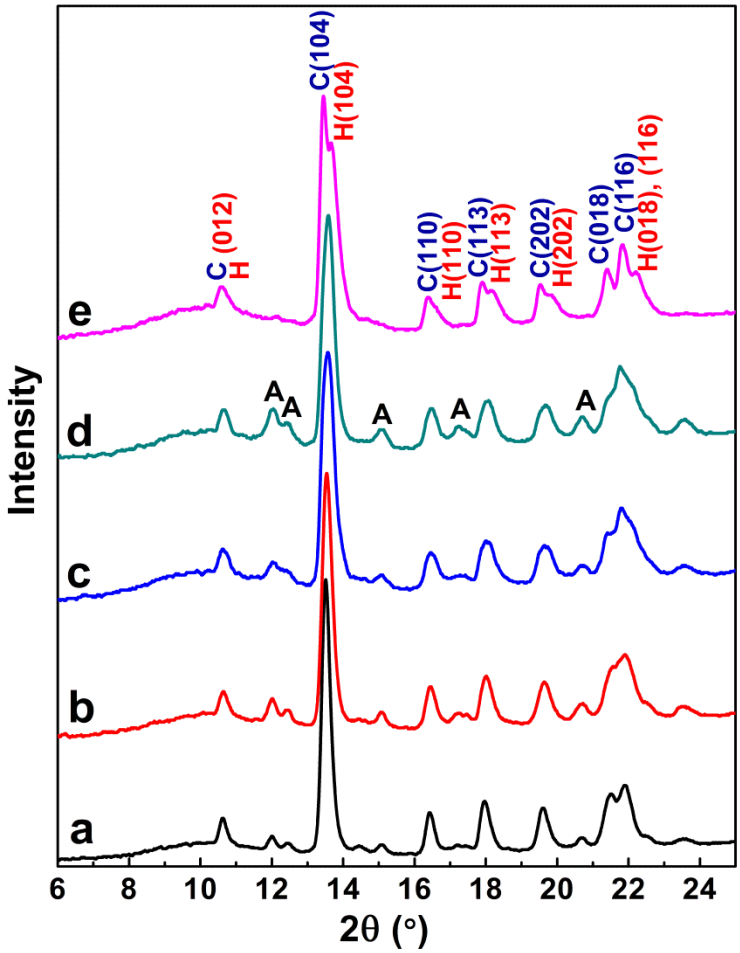

892

FIGURE 9. Comparison of the $MgCO_3$ contents of synthetic carbonates precipitated in control, non-metabolizing *H. saccharolyticum* or *D. retbaense* biomass-bearing solutions at different initial Mg:Ca ratios. $MgCO_3$ content in synthetic carbonates was determined based on the empirical curve (Zhang et al., 2010) correlating the $MgCO_3$ content and the shift of carbonate (104) peak toward dolomite (see Table 2). Error bars represent standard deviation of at least duplicate samples.

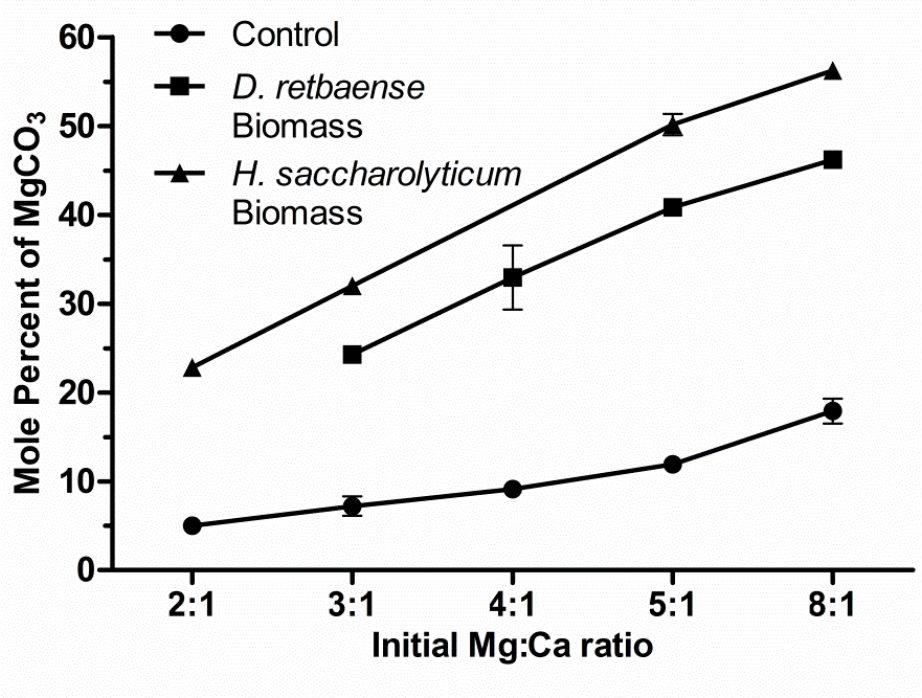

902 **FIGURE 10.** SEM and TEM examinations of synthetic carbonates.

903 (a): SEM image of Ca-Mg carbonate close to dolomite composition synthesized in consortium
904 bound EPS-bearing solutions.

905 (b): TEM image of Ca-Mg carbonate close to dolomite composition synthesized in bound EPS-
906 bearing solutions (initial Mg:Ca = 3:1) overgrowing a chalk seed. The "C" and "D" stand for the
907 chalk seed and Ca-Mg carbonates close to dolomite composition, respectively. Inset is an EDS
908 spectrum of the synthetic dolomite that contained ~52 mol% $MgCO_3$, which is consistent with
909 the high angle shoulder on high-Mg calcite (104) peak on the XRD pattern (Fig. 2d). Ca-Mg
910 carbonates close to dolomite composition occur as nano-crystals (~10-20 nm)

911 (c): SAED pattern of the chalk seed and Ca-Mg carbonate close to dolomite composition in (b).
912 The sharp spots are from the chalk seed since the *d*-spacing of the sharp (104) diffraction spot is
913 3.03 Å, which matches that of calcite. The diffraction arcs are from Ca-Mg carbonate close to
914 dolomite composition, since the *d*-spacing of the (104) diffraction arc is ~2.92 Å, which matches
915 that of Ca-Mg carbonate close to dolomite composition. The diffraction arcs suggest low-angle
916 grain boundaries among nano-crystals of Ca-Mg carbonates. However, the position of the
917 diffraction arcs followed that of the chalk seed, indicating that Ca-Mg carbonate close to
918 dolomite composition overgrew the chalk seed.

919 (d): High-resolution TEM image and a [010]-zone axis Fourier transform pattern (inset) from
920 Ca-Mg carbonates close to dolomite composition.

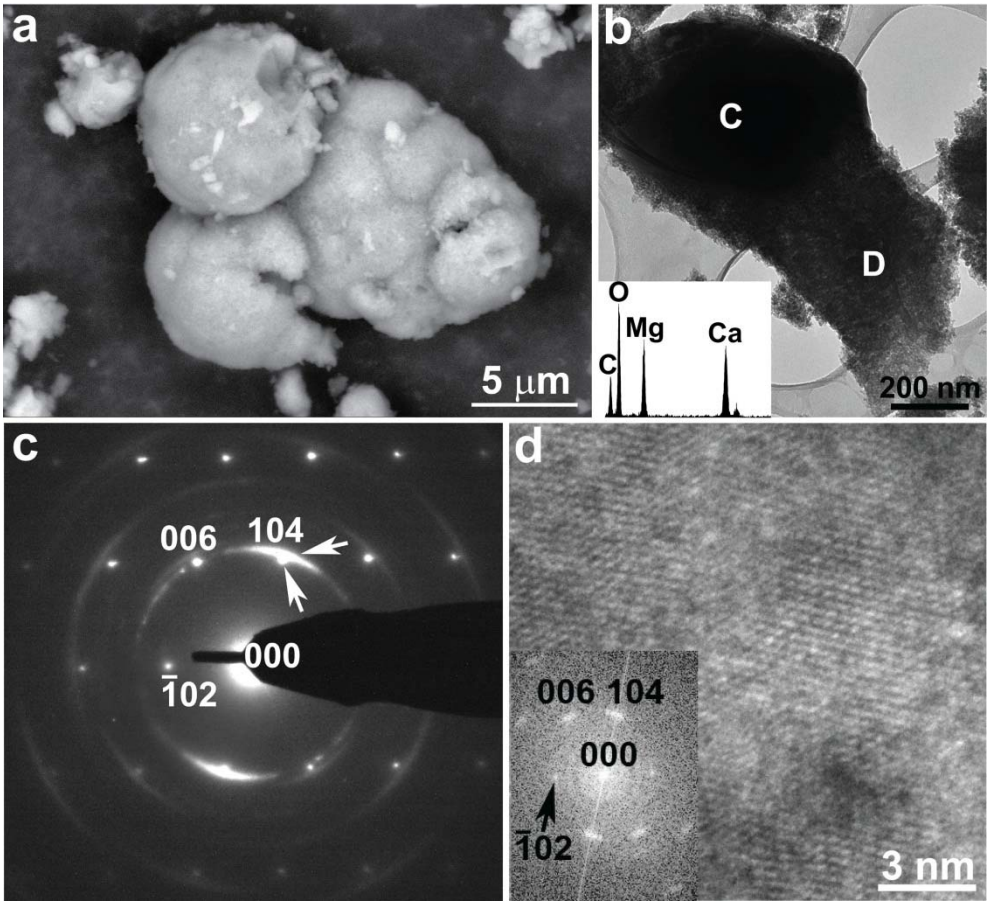

921

FIGURE 11. SEM images of synthetic carbonates.

(a): SEM image of synthetic rhombohedral calcite seeds.

(b): SEM image of high-Mg calcite clusters (~12 mol% $MgCO_3$) synthesized in control solutions containing synthetic seeds.

(c): SEM image of disordered Mg-rich dolomite (~57 mol% $MgCO_3$) synthesized in experimental solutions containing non-metabolizing *H. saccharolyticum* biomass and synthetic seeds. Disordered dolomite overgrew synthetic seeds, and the rhombohedral shape was overall preserved.

(d): A close up of the image in (c) shows that disordered dolomite occurred as extremely small nano-crystals.